FINAL REPORT

INVESTIGATION OF HORIZONTAL ION DENSITY GRADIENTS IN THE ATMOSPHERE

Contract NOnr 4969(00)

LMSC/L-39-70-1

FINAL REPORT

INVESTIGATION OF HORIZONTAL ION DENSITY GRADIENTS IN THE ATMOSPHERE

Contract NOnr 4969(00)

For Period

15 July 1965 through 29 May 1970

G. W. Sharp
R. D. Sharp
R. G. Johnson

This research was supported by the Advanced Research Projects Agency (ARPA Order 215) and was conducted under Office of Naval Research Contract NOnr 4969(00), Task No. 321-009.

Lockheed Palo Alto Research Laboratory
LOCKHEED MISSILES & SPACE COMPANY
Palo Alto, California

TABLE OF CONTENTS

LIST OF FIGURE CAPTIONS

LIST OF FIGURE CAPTIONS (continued)

LIST OF TABLES

ACKNOWLEDGMENTS

We wish to thank Mr. R. G. Joiner of the Office of Naval Research and Lt. Colonels J. K. Lerohl and J. Hill, USAF, of the VELA Office of the Advanced Research Projects Agency for organizing and providing direction to the program and for their persistent efforts required to obtain suitable satellite space for the payload. The cooperative support of Messrs. B. Zillgitt, J. Kitsos, K. Hultner and P. Smith of the General Dynamics Corporation, Convair Division, to the successful integration of this spectrometer with the OV1-18 spacecraft is hereby acknowledged. Special acknowledgment is made to Major J. McSherry, Colonel R. D. Spowart and Colonel W. B. Wilson of the Office of Aerospace Research, USAF, for their support throughout the integration, launch and orbital operations of the OV1-18 spacecraft. We acknowledge the support of the Advanced Research Projects Agency and the Office of Naval Research through Contract NOnr 4969(00).

Section 1

INTRODUCTION

This is the final report for a satellite measurement program to investigate the characteristics and causes of horizontal ion density gradients in the F-region ionosphere. The satellite payload was successfully launched on 18 March 1969 into a polar orbit and has been providing data since that time. This report covers the development of the payload, the satellite orbital operations, and the preliminary data analysis phases of the program. The analysis of the flight data is being continued under Contract N00014-70-C-0324.

The ionosphere is frequently characterized by its ability to absorb, refract, or reflect electromagnetic irradiations. These characteristics are clearly important to terrestrial and space communications networks and to radar tracking systems, particularly over-the-horizon tracking systems. In addition, the ionosphere plays an important role in the ability to detect, locate, and characterize nuclear detonations by means of the electromagnetic signals produced by the detonations. Changes in the natural ionospheric density and composition are also produced by nuclear detonations in or near the ionosphere, and identification of the perturbed ionization can serve as a means of detection and characterization of the nuclear device.

It is well known that nuclear detonations in the earth's magnetosphere produce strong electromagnetic signals, particularly in the low-frequency range. Detection of these signals and measurements of their characteristics provide a means of identifying, locating, and characterizing a nuclear detonation. Electromagnetic signals from nuclear detonations have frequently been observed at large distances from the point of detonation as a result of the propagation of the signals through the ionosphere or within the earth-ionosphere cavity. The intensity, time dependence, and frequency composition of these signals at remote distances are strong functions of the characteristics of the ionosphere. At present, our limited knowledge of the structure of the ionosphere continues to limit our ability to determine the electromagnetic source characteristics from measurements on the signals received at distant stations.

Prior to the initiation of the present program, large horizontal gradients in the ion density near the region of maximum density in the F-region (300-350 km) had been observed by the Lockheed Upper Atmospheres Group[1] with satellite instrumentation during a 4-day flight in November 1963. Some of the gradients persisted from day to day and were generally aligned with the magnetic field. These data, coupled with earlier data from the Alouette topside sounder, indicated that a nighttime trough of low ion density might be present at all altitudes on the equatorial side of the auroral zones. The data also showed that the ion density gradients on the nightside of the earth in the region of the polar auroral zones were related to the low-energy precipitated particle fluxes in those regions. Horizontal gradients were also observed in the South Atlantic anomaly region and they appeared to be directly associated with the artificial radiation belt and at times with the Van Allen radiation belt[2]. More detailed reports of the early Lockheed and Alouette results have subsequently been published elsewhere[3,4].

The present program was undertaken to improve our understanding of the horizontal ion density gradients. The major goals of the program are 1) to investigate the vertical extent of the type of horizontal ion density gradients observed in November 1963, 2) to study the local time dependence and other long-term and short-term variations of the observed structure and 3) to investigate the role of the energetic particle fluxes in providing the ion density gradients.

Initially, two satellite flights were planned. One was to be flown above the F-region peak density (400-500 km) and one below the peak (250-300 km). The satellite experiment that has been completed and is reported here was flown above the F-peak.

The satellite was launched on 18 March into a 99° inclination orbit with apogee initially at 590 km and the perigee at 469 km. All of th payload performed well on orbit initially and most of it continued to perform well throughout the first year's operation. The satellite, however, failed to achieve orientation and tumbled in a near random fashion but with a tumble

rate that varied with time. In spite of this failure, all of the instrumentation provided some high-quality data and a large body of data has been acquired that promises to yield significant results on the systematic relationships between the ionospheric structure at this altitude and the input energy sources in the form of particle fluxes. Electron density and temperature measurements with the Langmuir probe were acquired throughout the experiment and ion density and temperature measurements were acquired during the first 225 orbits. The preliminary analysis has shown that ionospheric structure is observed and is significant at this altitude. The failure of the satellite to achieve stabilization has complicated the analyses, and the delay in obtaining good ephemeris data from the Air Force for the period prior to orbit 388 has resulted in a delay in the analysis of the ion and electron density data since detailed attitude information is required for the interpretation of the data.

Substantial progress has been made in the preparation of a series of computer programs for processing the flight data. These programs have been used in the analysis of the particle flux data to verify their applicability to flight data of varying quality, and detailed surveys of the particle fluxes for some of the early orbits have been performed.

Section 1

REFERENCES

1. Sharp, G. W., T. J. Crowther and C. W. Gilbreth, "Some Recent Ion Concentration Measurements Obtained from a Polar-Orbiting Satellite," Trans. Am. Geophys. U., 45, 87-88 (1964).

2. Sharp, G.W., W. L. Imhof and R. G. Johnson, "Direct Evidence for Corpuscular Radiation Effects on the Ionosphere in the Southern Anomaly Region," COSPAR Conference, Buenos Aires, May 1965; Space Research VI, North-Holland Pulbishing Co., 1966.

3. Muldrew, D. B., "F-Layer Ionization Troughs Deduced from Alouette Data," J. Geophys. Res., 70, 2635 (1965).

4. Sharp, G. W., "Midlatitude Trough in the Night Ionosphere," J. Geophys. Res., 71, 1345 (1966).

Section 2

INSTRUMENTATION

2.1 Ionospheric Measurements

The state of the ionosphere is best described in terms of the ion density, ion temperature, electron density, electron temperature and the intensity and distribution of epithermal electron fluxes. In this investigation of the horizontal ion density gradients in the lower ionosphere these parameters have been measured. The accomplishment of this task has been obtained with the following instrumentation: an Ion Energy Analyzer (IEA) to measure ion densities and temperatures; an Epithermal Electron Analyzer (EEA) to measure the intensity and distribution of epithermal electron fluxes; and a cylindrical Langmuir probe to measure electron densities and temperatures.

The Ion Energy Analyzer (IEA) flown in this experiment was a retarding potential analyzer which operated in the range from +27 volts to -10 volts. The sweep voltage changed lineurly from +27 volts to -10 volts in a two-second period and the return sweep was accomplished in a one-second period. The IEA had the capability of measuring the ion densities of two different groups of ions in an ionosphere composed of two groups, namely molecular ions (NO^+, O_2^+, N_2^+, etc.) and atomic ions (O^+, N^+, etc.). In addition to the separate ion densities the common ion temperature is also obtained. The data is partially "on-board" processed such that very little telemetry bandwidth is used in transmitting the data. A complete description of the operation of a similar instrument is given in the literature[1].

The particular model of the IEA in this experiment required last-minute modifications due to the change in the stabilized orientation of the vehicle. The IEA is designed to be oriented looking into the velocity vector. Inasmuch as the vehicle was projected to be relatively unstable around the yaw axis, the sensor elements of the IEA were increased from initially one to four. These elements were located on the

vehicle such that in the two axes stabilized condition at least one of the sensor elements would be nearly in the direction of the velocity vector.

The instrument with the four sensor elements was carefully calibrated for each mode of operation. A typical calibration curve is shown in Figure 2.1. The figure is a reproduction of an actual strip chart record of a calibration run. The various channels of the chart are labeled corresponding to the functions of the instrument. The basic cycle of the instrument is demonstrated by the "sweep" channel.

A conventional cylindrical Langmuir probe was supplied through the courtesy of Professor A. Nagy of the University of Michigan. This instrument measures the electron concentration and the electron temperature by applying a negative retarding sweep potential to a cylindrical wire probe. The electrons collected on the probe are then analyzed. From the characteristic volt-ampere curve the electron density and temperature may be obtained. A more detailed discussion of this type of instrument and the data analysis may be found in the literature[2].

The Epithermal Electron Analyzer (EEA) experiment was incorporated in the satellite to measure the flux of electrons as a function of energy in the range 0-128 electron volts. Electrons in this energy range are produced by photoionization of the neutral atmosphere, by energetic particle bombardment of the neutral atmosphere, and by other processes such as joule heating and heat conduction from the magnetosphere. These low energy electrons are potentially responsible for exciting many of the airglow lines such as 1493-A of atomic nitrogen, and the 1304-, 1356-, 5577- and 6300-A lines of atomic oxygen. They also play an important role in the energy degradation of extreme ultraviolet photons and energetic particles into thermal energy of the upper atmosphere.

An example of one of the sensors attached to the electronics box is illustrated in Figure 2.2. The cylindrical portion contains grids and a collector which together serve to exclude the positive ions in the ionosphere and to collect negatively charged particles (essentially all electrons)

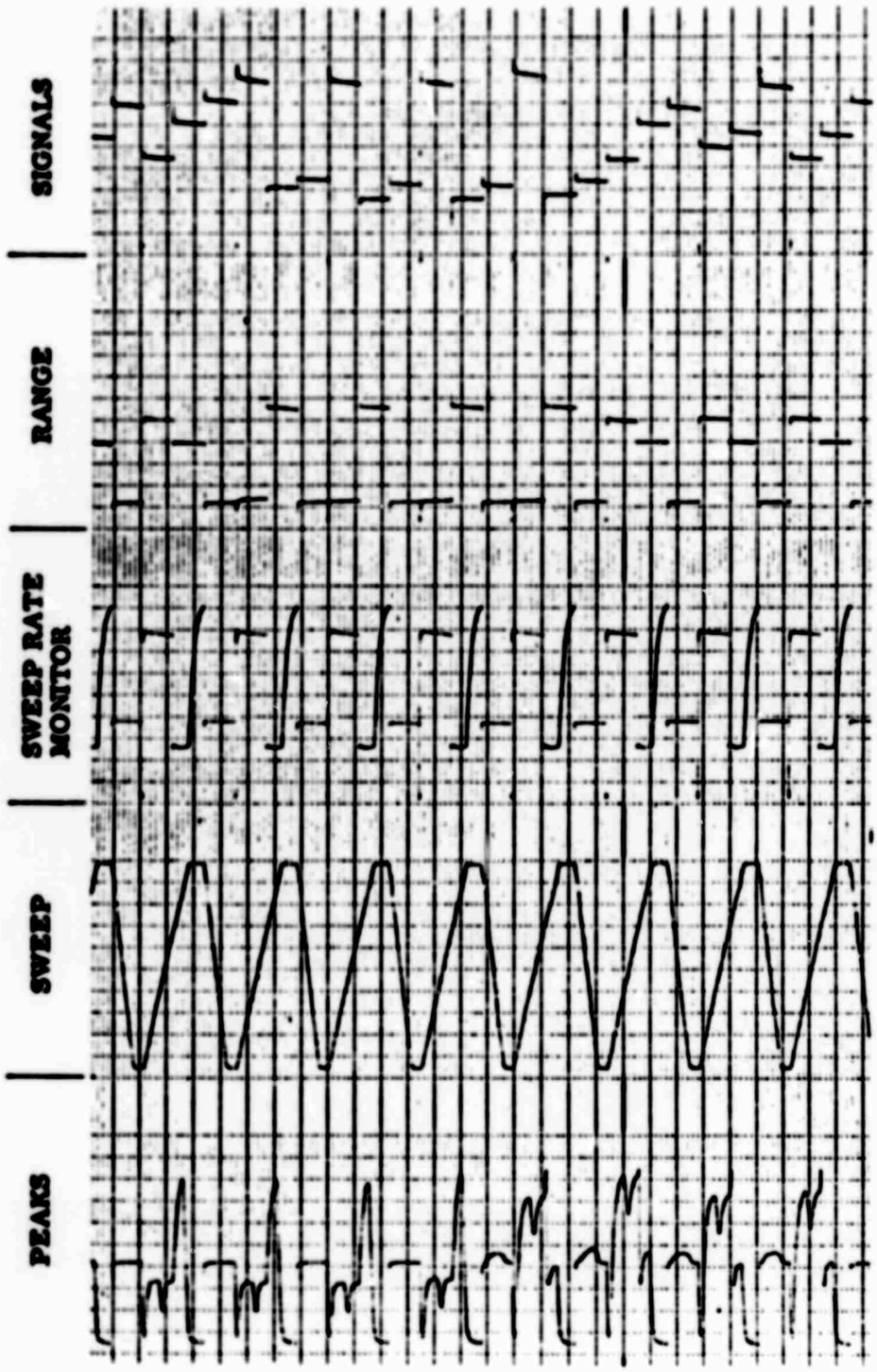

Figure 2.1 Calibration record for Ion Energy Analyzer.

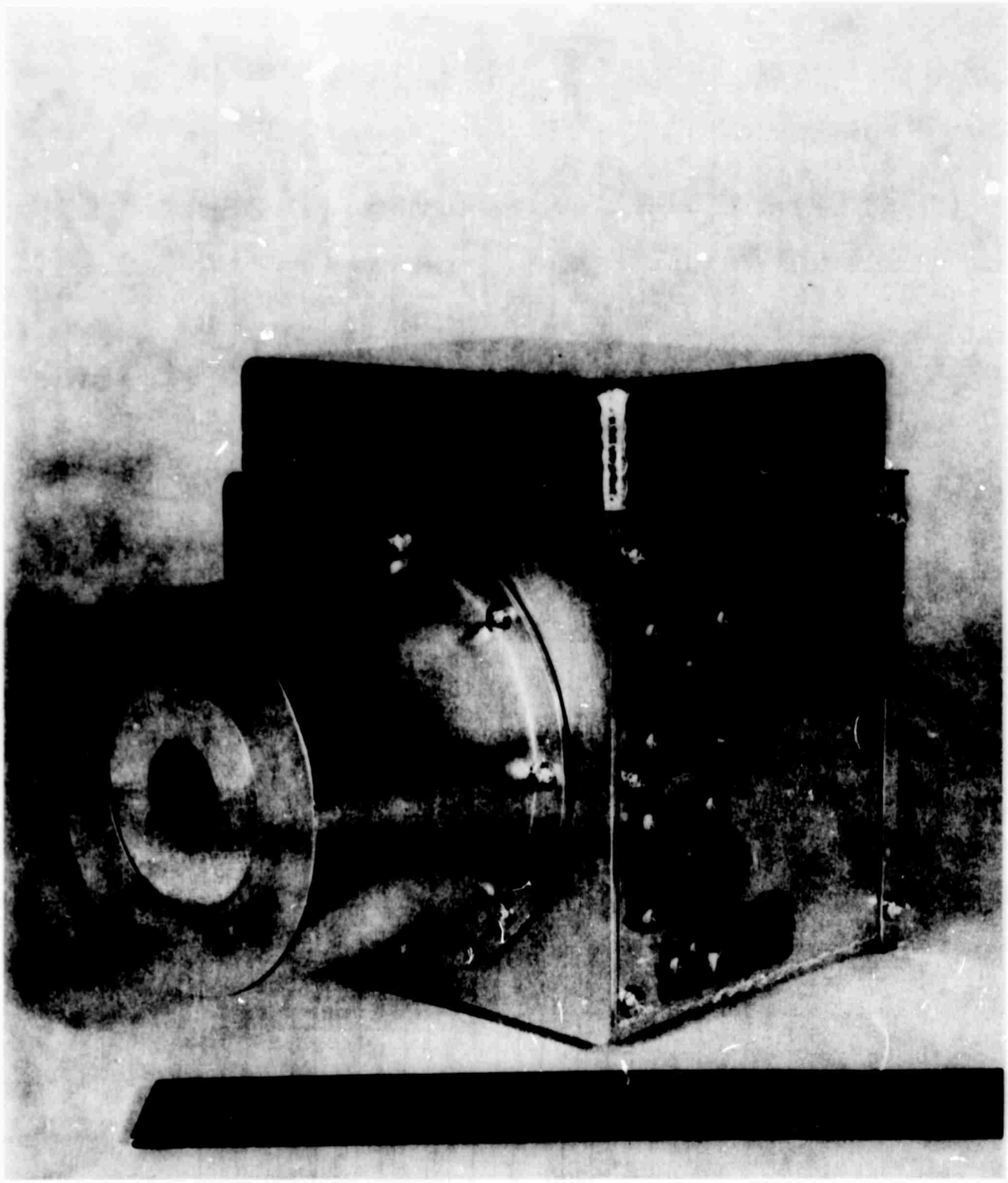

Figure 2.2 One of the epithermal electron analyzer sensors.

which have sufficient energy to penetrate the retarding potential barrier established on one of the grids. The retarding potential is stepped successively from zero to 128 volts to determine the flux in eight energy intervals.

Three sensors were mounted on the satellite in different orientations, two of them antiparallel. The three sensors were required to overcome electron shadowing by the vehicle in the earth's magnetic field. The two detectors which were antiparallel permit measurement of a resultant electron current along the magnetic field line.

The sensors were designed to measure the flux over the range 10^5-10^{11} particles/cm^{-2}-sec^{-1}-$ster^{-1}$. Figure 2.3 is the calibration curve for sensor 1 and demonstrates that this range was successfully achieved. Preliminary data analysis indicates that the electron fluxes fell within the range of the sensors at essentially all times.

2.2 Particle Detectors

An array of low-energy particle detectors was included in the payload in order to adequately document the energy inputs to the ionosphere from low-energy precipitation events. The angular distributions, energy distributions, spatial and temporal distributions of low-energy particle precipitations are known to be highly variable and the fluxes can be in the form of electrons, protons or energetic Helium ions. Sufficient instrumentation is required to define all of the many parameters in the event. We have chosen two complementary forms of instruments to perform these measurements. The first type uses a scintillator-photomultiplier combination as the detecting element. It can be made with a large geometric factor and so can obtain an adequate statistical sampling in a relatively short time and is therefore particularly suited for studying narrow auroral structures and fast temporal changes in the precipitation. The energy and particle type is determined by some combination of electrostatic, magnetic, and foil threshold analysis. The design considerations and a detailed discussion of the construction and calibration of this type of

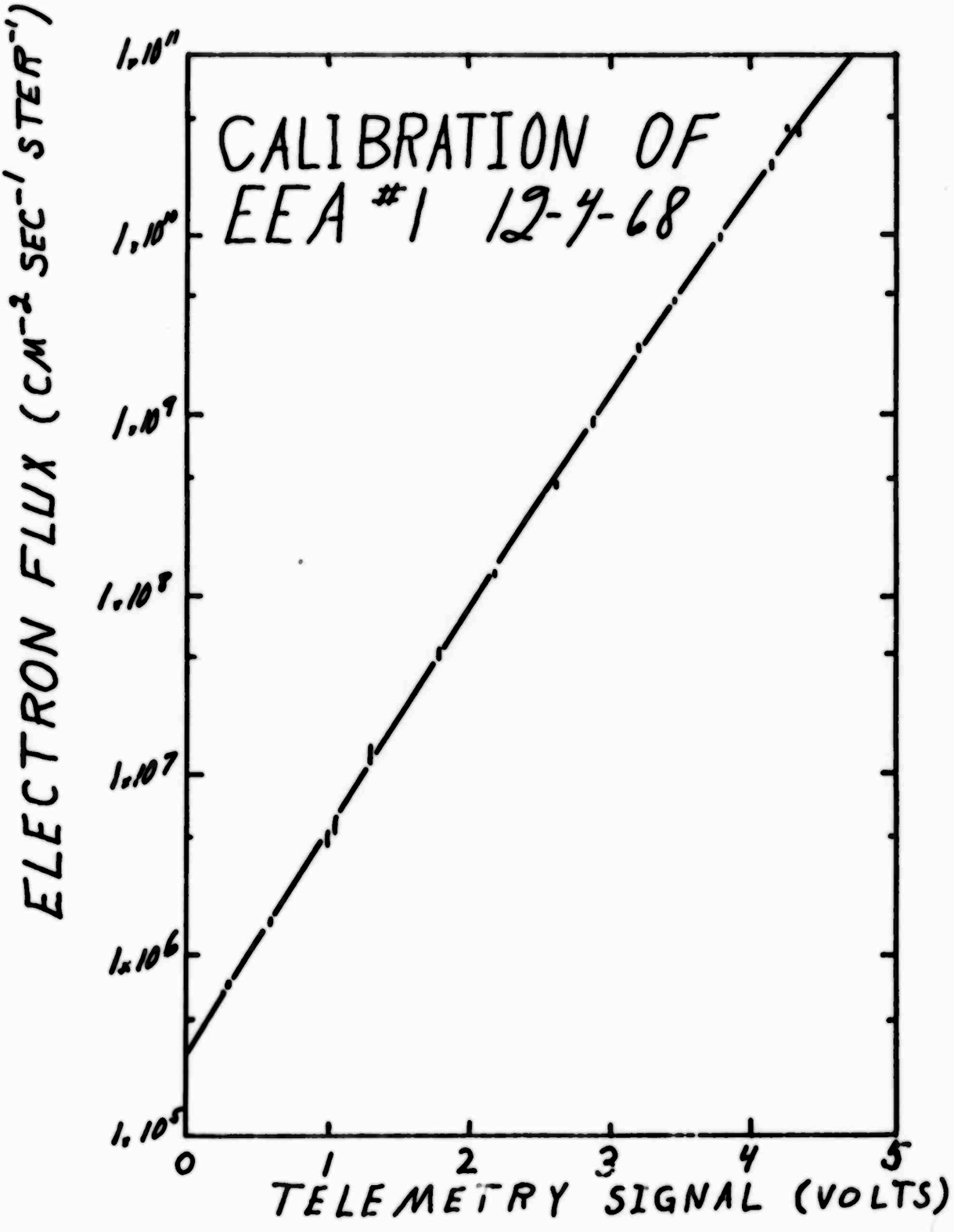

Figure 2.3 Calibration curve for one of the epithermal electron analyzers.

instrument has been published[3,4]. Five of them have been included in the payload. Angular Distribution Instruments (ADI) -1, -2 and -3 measure the angular distribution of the total energy flux above two thresholds (0.2 and 1.2 keV) by means of a variable electrostatic threshold which is cycled eight times per second between the two values indicated. Two instruments, Total Energy Proton (TEP) detectors -1 and -2, measure the total proton energy flux above 4 keV and the total energetic electron flux (electrons above 21 keV). The threshold values for these instruments are defined by thin evaporated aluminum foils on the faces of the scintillators and the electrons are separated from the heavy ions with magnetic analysis. The geometric factors, angular ranges and other specific characteristics of the several flight instruments are shown in Table 2-1. The second basic type of instrument used is based on the Channel-Electron-Multiplier (CEM) as the detecting element. These detectors are very compact and so many channels can be included in the payload, allowing one to achieve good energy resolution. The small detector size, however, limits the statistical accuracy of the measurements in weak or rapidly varying events. In this sense they are complimentary to the scintillator-photomultiplier detectors described above. We have included five instruments of this type in the payload, oriented in different directions so as to perform an angular distribution measurement of the incident flux. Each instrument contains from six to ten modular channels and each channel measures a specific energy group of either electrons or protons. The channels are essentially independent detectors consisting of a CEM as the sensor and some combination of magnetic and/or foil threshold analysis to define the energy range and the type of particle. The modular channels are stacked together in groups of from six to ten on a base which contains a common high-voltage supply and signal handling circuitry. The design, construction and calibration of these instruments has been described in the literature[5] and will not be elaborated upon here.

The individual modules can be one of several types. The CME (Channel-electron-multiplier - Magnetic analysis - Electrons) uses a 180° permanent magnet spectrometer to define the energy range. The CMP (Channel-electron

Name	Detector*	Analysis†	Particles Measured**	Energy Range (keV)	Geometric Factor (cm^2-ster)	Nominal Pointing Angle (with Respect to Zenith)	Angular Acceptance Full Angle in Degrees)	Sensitivity Threshold (Particles/ cm^2-sec-sr)
CFP-1B	C	F,MB	P	>10	1.3×10^{-4}	0°	13.6	2.7×10^{4}
CFP-1D	C	F,MB	P	>25	1.3×10^{-4}	0°	13.6	2.5×10^{4}
CME-1A	C	M	E	0.8-1.5	8.7×10^{-6}	0°	10x10	4.4×10^{5}
CME-1B	C	M	E	1.75-3.3	8.1×10^{-6}	0°	10x10	3.2×10^{5}
CME-1C	C	M	E	3.75-7.0	9.6×10^{-6}	0°	10x10	3.2×10^{5}
CME-1D	C	M	E	8.3-16.3	2.6×10^{-5}	0°	10x10	3.2×10^{4}
CME-1E	C	M	E	17.3-37	4.0×10^{-5}	0°	10x10	9.7×10^{4}
CME-1F	C	M	E	Background	-	0°	-	5.6×10^{4}
CXA-1A	C	EA,X	A	1	3.0×10^{-4}	0°	10x10	3.3×10^{4}
CXA-1B	C	EA,X	A	3	3.0×10^{-4}	0°	10x10	3.3×10^{4}
CXA-1C	C	EA,X	A	8	3.0×10^{-4}	0°	10x10	3.3×10^{4}
ADI-1	P	ET	E	>0.2, >1.2	2.0×10^{-1}	0°	40	3.3×10^{6}††
CMP-3A	C	M	P	0.25-1.75	2.5×10^{-5}	55°	16x6	5×10^{4}
CMP-3B	C	M	P	0.75-5.25	2.5×10^{-5}	55°	16x6	8.3×10^{4}
CMP-3C	C	M	P	2.0-14.0	2.5×10^{-5}	55°	16x6	9.3×10^{4}
CFP-2A	C	F,MB	P	>4	3.25×10^{-5}	55°	12.6	1.7×10^{5}
CFP-3B	C	F,MB	P	>10	3.25×10^{-5}	55°	12.6	1.2×10^{5}
CFP-2C	C	F,MB	P	>25	1.3×10^{-4}	55°	13.6	1.2×10^{5}
CFP-3D	C	F,MB	P	>50	1.3×10^{-4}	55°	13.6	2.6×10^{4}
CFP-2E	C	F,MB	P	>1000	1.3×10^{-6}	55°	13.6	3.2×10^{4}
CME-2A	C	M	E	0.80-1.5	7.5×10^{-6}	55°	10x10	7.6×10^{5}
CME-3B	C	M	E	1.8-3.3	8.4×10^{-6}	55°	10x10	3.4×10^{5}
CME-3C	C	M	E	3.75-7.0	9.8×10^{-6}	55°	10x10	3.2×10^{5}
CME-2D	C	M	E	8.2-16.5	2.2×10^{-5}	55°	10x10	2.4×10^{5}
CZU-2	C	-	U	-	-	55°	-	1.3×10^{5}
ADI-2	P	ET	E	>0.2, >1.2	2.0×10^{-1}	55°	40	- 5×10^{6}††
TEP-108-1	P	F,MB	P	>4	2.0×10^{-1}	55°	40	5×10^{5}††
TEP-108-2	P	F	E	>21	2.0×10^{-5}	55°	40	1.2×10^{4}††
CFP-4B	C	F,MB	P	>10	6.5×10^{-5}	55°	12.6	6×10^{4}
CFP-4D	C	F,MB	P	>25	6.5×10^{-5}	55°	13.6	7.0×10^{4}
								3.0×10^{4}

Table 2-I. CHARACTERISTICS OF LOW-ENERGY PARTICLE DETECTORS (Sheet 1)

Table 2-I. CHARACTERISTICS OF LOW-ENERGY PARTICLE DETECTORS (Sheet 2)

Name	Detector*	Analysis†	Particles Measured**	Energy Range (keV)	Geometric Factor (cm^2-ster)	Nominal Pointing Angle (with Respect to Zenith)	Angular Acceptance (Full Angle in Degrees)	Sensitivity Threshold (Particles/cm^2-sec-sr)
CME-4A	C	M	E	0.8-1.5	7.6×10^{-6}	90°	10x10	4.1×10^{5}
CME-4B	C	M	E	1.8-3.25	9.4×10^{-6}	90°	10x10	2.8×10^{5}
CME-4C	C	M	E	3.7-7.0	8.5×10^{-5}	90°	10x10	3.5×10^{4}
CME-4D	C	M	E	8.4-16.3	2.5×10^{-4}	90°	10x10	7.0×10^{4}
CFE-4A	C	F	E	>2	3.8×10^{-4}	90°	40	2.6×10^{4}
CFE-4B	C	F	E	>10	3.8×10^{-4}	90°	40	2.6×10^{4}
CFE-4C	C	F	E	>60	3.8×10^{-4}	90°	40	2.6×10^{6}††
ADI-3	P	ET	E	>0.2, >1.2	8.5×10^{-3}	90°	40	5×10^{3}
CFP-5B	C	F,MB	P	>10	9.0×10^{-4}	180°	18.6	3.5×10^{3}
CFP-5C	C	F,MB	P	>25	9.0×10^{-4}	180°	18.6	2.7×10^{3}
CFP-5D	C	F,MB	P	>50	3.5×10^{-3}	180°	21.4	7.9×10^{3}
CFP-5E	C	F,MB	P	>1000	3.5×10^{-3}	180°	21.4	2.8×10^{5}
CME-5A	C	M	E	0.6-1.8	3.6×10^{-5}	180°	16x10	1.3×10^{5}
CME-5B	C	M	E	1.75-5.3	3.5×10^{-5}	180°	16x10	1.8×10^{5}
CME-5C	C	M	E	5.0-16.0	4.9×10^{-5}	180°	16x10	1.3×10^{5}
CME-5D	C	M	E	14.0-48.0	1.6×10^{-4}	180°	16x10	5.2×10^{4}
CZU-5	C	-	U	-	-	180°	-	-
CFE-5	C	F	E	>40	3.5×10^{-3}	180°	21.4	2.8×10^{3}

* C = Channeltron
P = Photomultiplier
PRM = Penetrating Radiation Monitor (See Text)

† EA = Electrostatic Analyzer
ET = Electrostatic Threshold
M = Magnetic Energy Analyzer
MB = Magnetic Broom (Removes Electrons)
F = Foil Threshold
X = Crossed Fields, Velocity Filter

†† Sensitivity Threshold (keV/cm^2-sec-sr)

** E = Electrons
P = Protons or hydrogen and heavier mass components
A = He^{++}, He^{+}, H^{+} (different masses resolved)
U = Ultraviolet background

multiplier - Magnetic analysis - Protons) also uses magnetic analysis but measures incident protons. The CFP (Channel-electron-multiplier - Foil threshold analysis - Protons) uses a magnetic broom to sweep out electrons and defines the threshold energy of the measured proton flux with a thin carbon or nickel foil. The CFE (Channel-electron-multiplier - Foil threshold analysis - Electrons) is a similar unit without the magnetic broom so that the difference between its response and that of the CFP gives the electron flux above the foil determined threshold. The CZU (Channel-electron-multiplier - Z [unspecified analysis] - Ultraviolet) is a background channel which measures the incident ultraviolet radiation in the 1000Å range. The channel-electron-multipliers are quite sensitive in this wave length region which contains both an intense solar line (1216Å) and several auroral emissions, and the background measurements are needed to subtract out this UV response when necessary. The specific characteristics of the individual channels included in the payload are shown in Table 2-I.

In addition to the five modular CEM instruments, an instrument has been included in the payload using CEM's as the sensing element, which is designed to measure the ratio of energetic Helium ions to protons in the auroral precipitations. It contains three channels each of which consists of a velocity filter (crossed electric and magnetic fields) in series with an electrostatic analyzer. The electrostatic analyzer is operated at a fixed energy (1, 3 or 8 keV in each of the three channels) and the electric field on the velocity filter is swept so that a range of mass-per-unit-charge is analyzed. The instrument is capable of resolving H^+, He^{++} and He^+ ions. Figure 2.4 shows the data from the 8-keV channel for two consecutive mass sweeps during an auroral precipitation event in the southern hemisphere which contained a substantial component of He^{++}.

As has been indicated, a substantial fraction of the low-energy detectors utilize thin foils to define the energy range of the particles measured. The precise determination of the thickness of these foils is required as part of the calibration process. This is accomplished by means of a thin radioactive source of Am^{241} which emits alpha particles of 5.48 MeV. A high-resolution solid-state detector is used to measure the energy loss of

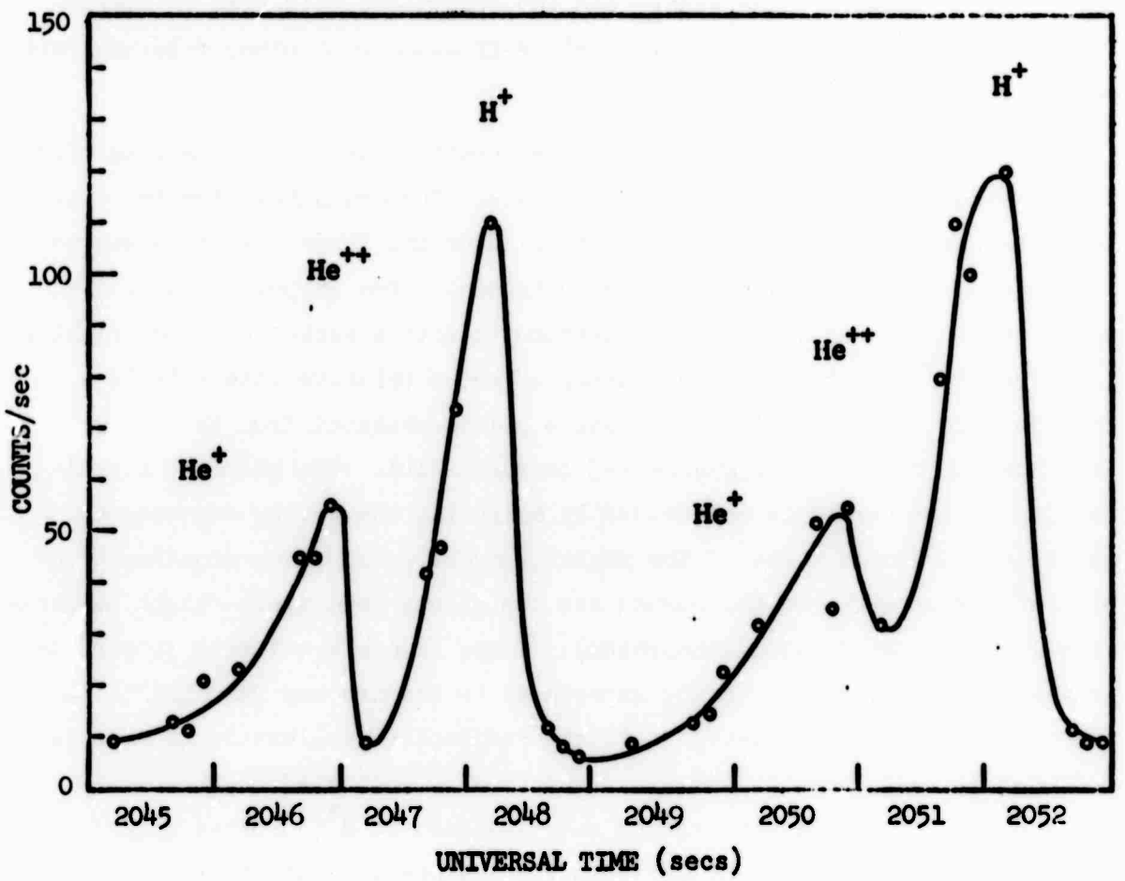

Figure 2.4 Flight data from the CXA (Channel-electron-multiplier - X [crossed-field analyzer] - Alpha particles plus protons). Two consecutive mass sweeps are indicated from a crossing of the auroral zone on 13 May 1969.

the alpha particles in traversing the foils. For the scintillator-photomultiplier detectors where the foil is evaporated directly onto the face of the scintillator, this is accomplished by determining the increased energy loss of the alpha particles in traversing a thin plastic film (formvar) which has been placed next to the scintillator during the evaporation process. These measured energy loss values and the equivalent thickness in $\mu gm/cm^2$ for the flight foils are given in Table 2-II along with other relevant foil parameters.

Figures 2.5 through 2.9 give the calibration curves for the five scintillator-photomultiplier flight instruments. The ordinates give the total particle energy deposition in the scintillator and the abscissas show the corresponding output voltage of the instrument. The shapes of the curves are determined by activating the instruments with a series of geometrically identical Sr^{90}-Y^{90} radioactive sources of known relative intensity in a reproducible geometry. The calibration points obtained from these sources are shown on the curve (labeled 2-3 through 2-12). The absolute normalization of the curves is determined by measuring the energy deposition in the scintillator from one of the weaker sources using pulse-counting techniques[3]. Also shown on the curves are the points from the in-flight calibration light diodes (Gallium-phosphide). These lights are turned on periodically during the course of the experiment to measure any gain drifts in the instruments. A low-level in-flight radioactive calibration source is included in each detector and its level is also indicated on the curves. For the ADI instruments the source material used is H^3(adsorbed in Zr) which has a beta spectrum of sufficiently low energy that it is affected by the repelling and post-acceleration voltages used in the instrument. The instrument response to the source in each of its two operating modes (200 eV and 1200 eV threshold steps) is indicated by the upper two points and the response in a possible failure mode (post acceleration and repeller voltages = 0) is shown as the lowest point.

Figures 2.10 and 2.11 give two representative calibration curves for the CEM instruments. The ordinates give the counting rate and the abscissas show the corresponding output voltages. Two curves are shown - one for

Table 2-II. CHARACTERISTICS OF FLIGHT FOILS

Instrument	Foil Number	Foil Material	Foil Diameter (inches)	Measured Foil Thickness		Light Transmission
				keV	$\mu gm/cm^2$	
ADI-1	129A	Aluminum	1.550	11.8	20.1	7.8×10^{5} **
ADI-2	129B	Aluminum	1.550	11.8	20.1	3.5×10^{6} **
ADI-3	129D	Aluminum	1.550	11.8	20.1	1.1×10^{6} **
TEP-108-1	602B	Aluminum	0.875	9.4	15.8	1.6×10^{7} **
TEP-108-2	113B	Aluminum†	0.875	13.0	22.0	6.1×10^{6} **
TEP-108-2	X6501A	Aluminum	0.705	-	1000*	-
CFP-1B	190	Nickel	0.028	26.4	61.5	1.4×10^{-3} Δ
CFP-1D	225	Nickel	0.028	95.5	222.0	$\leq 4.1 \times 10^{-7}$ Δ
CFP-2A	143	Carbon	0.014	10.4	13.7	1.2×10^{-2} Δ
CFP-2C	264	Nickel	0.028	56.0	130.0	$\leq 2.4 \times 10^{-7}$ Δ
CFP-2E	215	Nickel	0.028	-	4150*	-
CFP-3B	186	Nickel	0.014	24.2	56.3	1.6×10^{-3} Δ
CFP-3D	234	Nickel	0.028	95.5	222.0	$\leq 7.2 \times 10^{-7}$ Δ
CFE-4A	255	Nickel	0.020	34.2	79.7	1.2×10^{-3} Δ
CFE-4B	232	Nickel	0.020	50.9	218.0	$\leq 9.5 \times 10^{-7}$ Δ
CFE-4C	221	Nickel	0.020	-	4150*	-
CFP-4B	254	Nickel	0.020	33.6	78.4	1.4×10^{-3} Δ
CFP-5D	231	Nickel	0.020	93.5	217.0	$\leq 4.3 \times 10^{-7}$ Δ
CFE-5	241	Nickel	0.110 mesh	-	2840*	-
CFP-5B	193	Nickel	0.056	25.9	60.3	1.5×10^{-3} Δ
CFP-5C	5	Nickel	0.056	65.4	151.5	$\leq 1.8 \times 10^{-7}$ Δ
CFP-5D	229	Nickel	0.110 mesh	96.0	223.0	1.7×10^{-6} Δ
CFP-5E	219	Nickel	0.110	-	4150*	-

* Weighed on microbalance

** Response to full moonlight (keV/sec of equivalent flux)

Δ Measured transmission fraction for 1216Å radiation

† An additional foil consisting of a layer of $\frac{1}{4}$-mil mylar with about 100 $\mu gm/cm^2$ Al evaporated on it is used in series with the foil evaporated on the scintillator for this instrument.

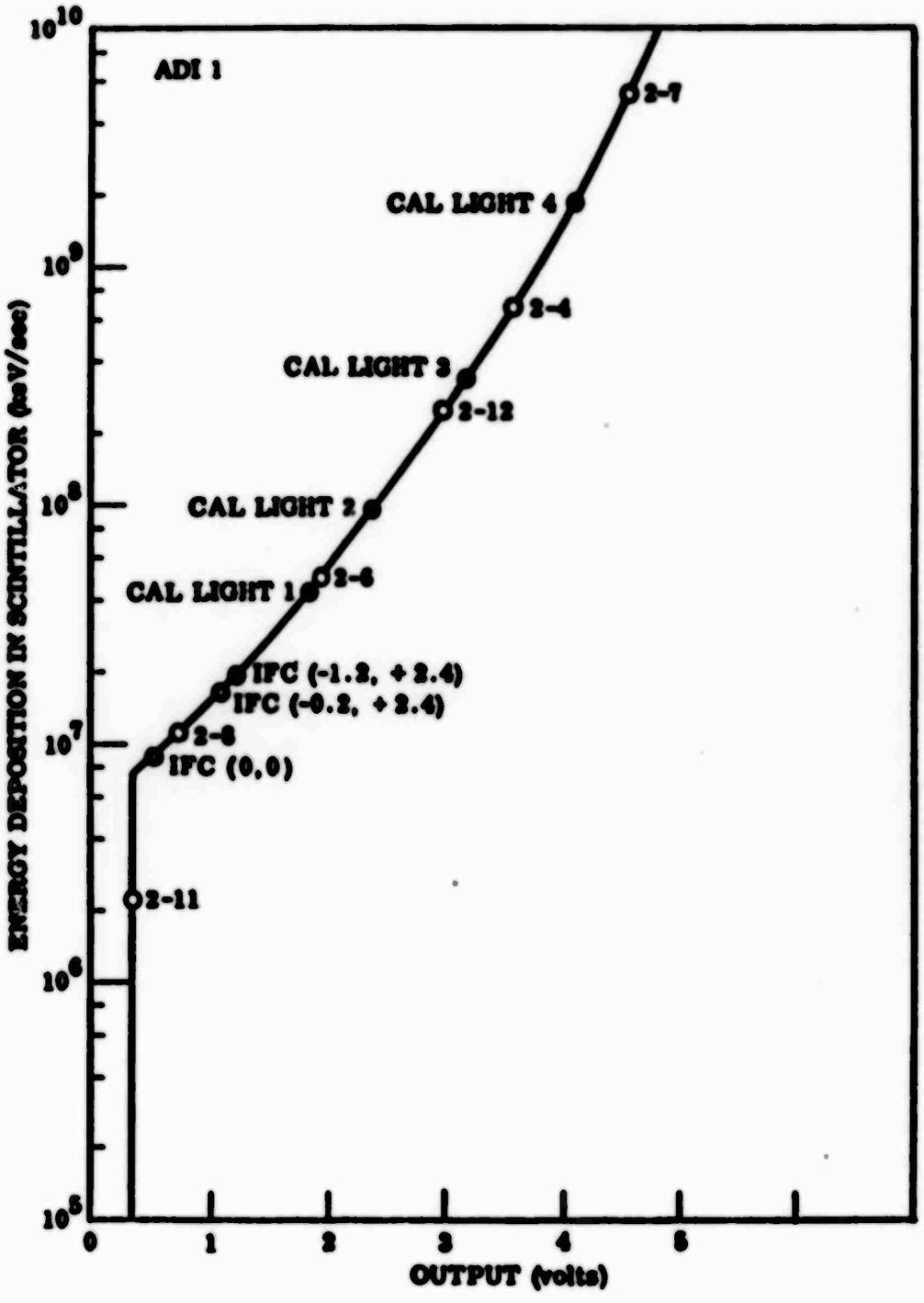

Figure 2.5 Calibration curve for ADI-1.

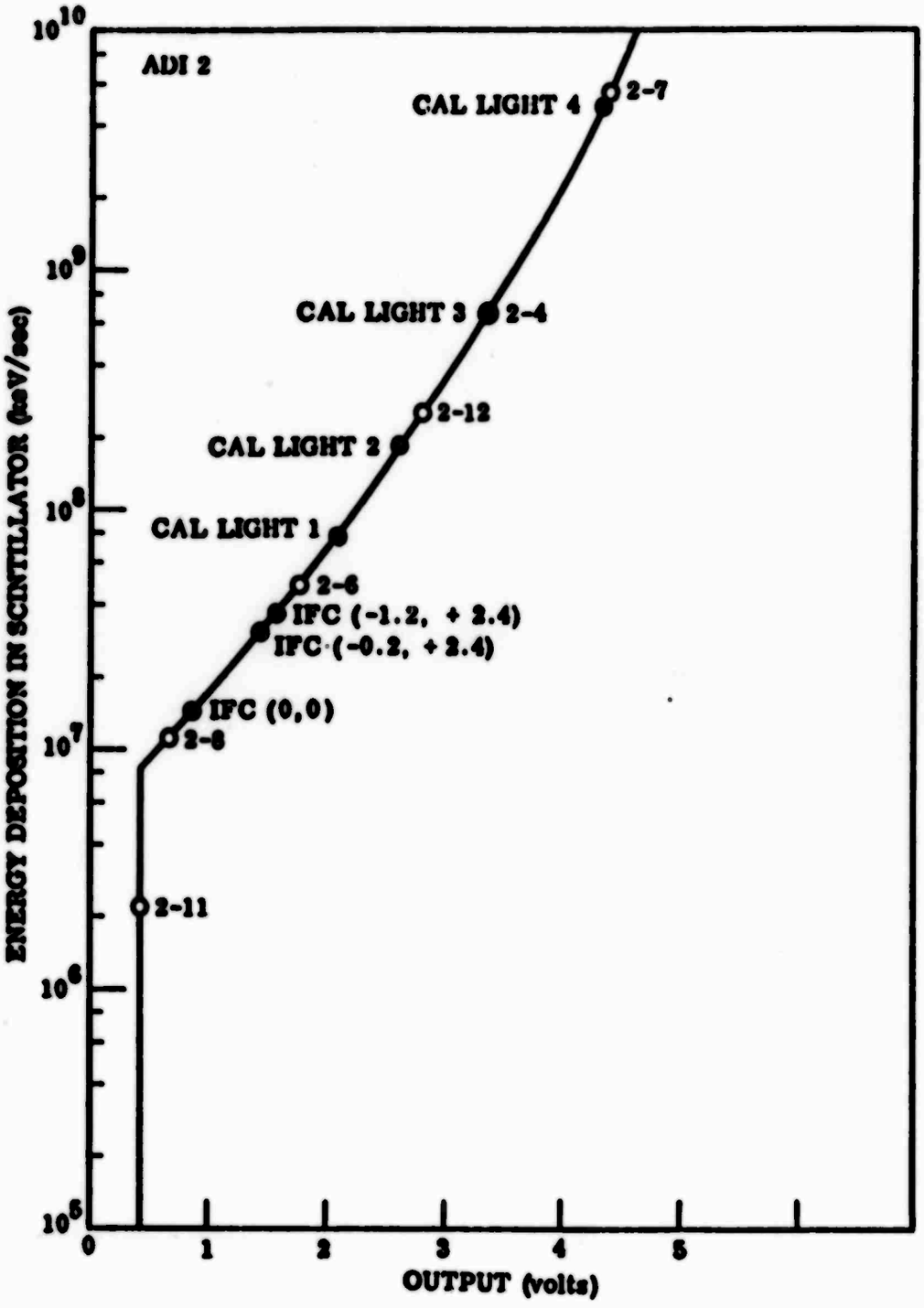

Figure 2.6 Calibration curve for ADI-2.

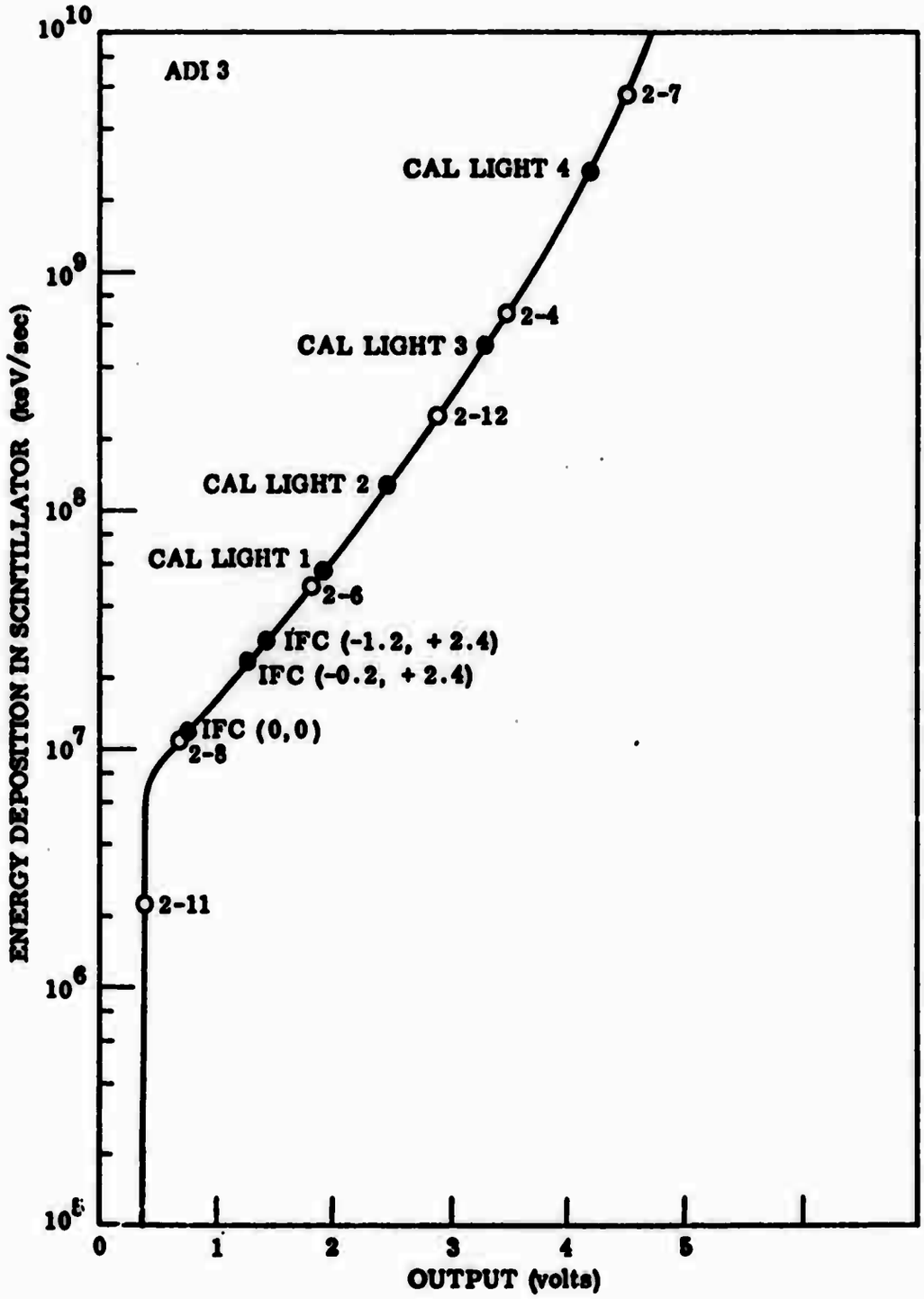

Figure 2.7 Calibration curve for ADI-3.

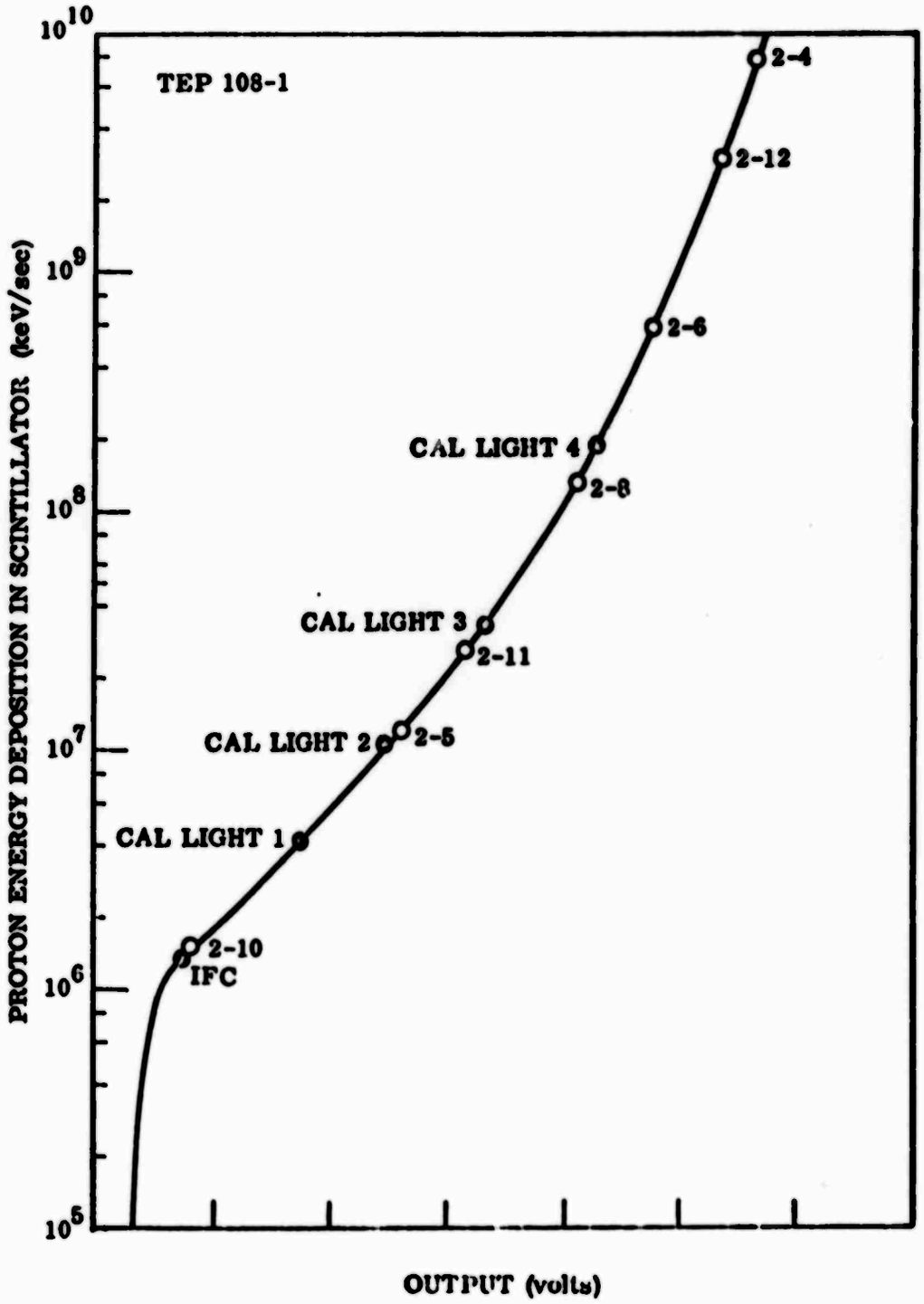

Figure 2.8 Calibration curve for TEP-1.

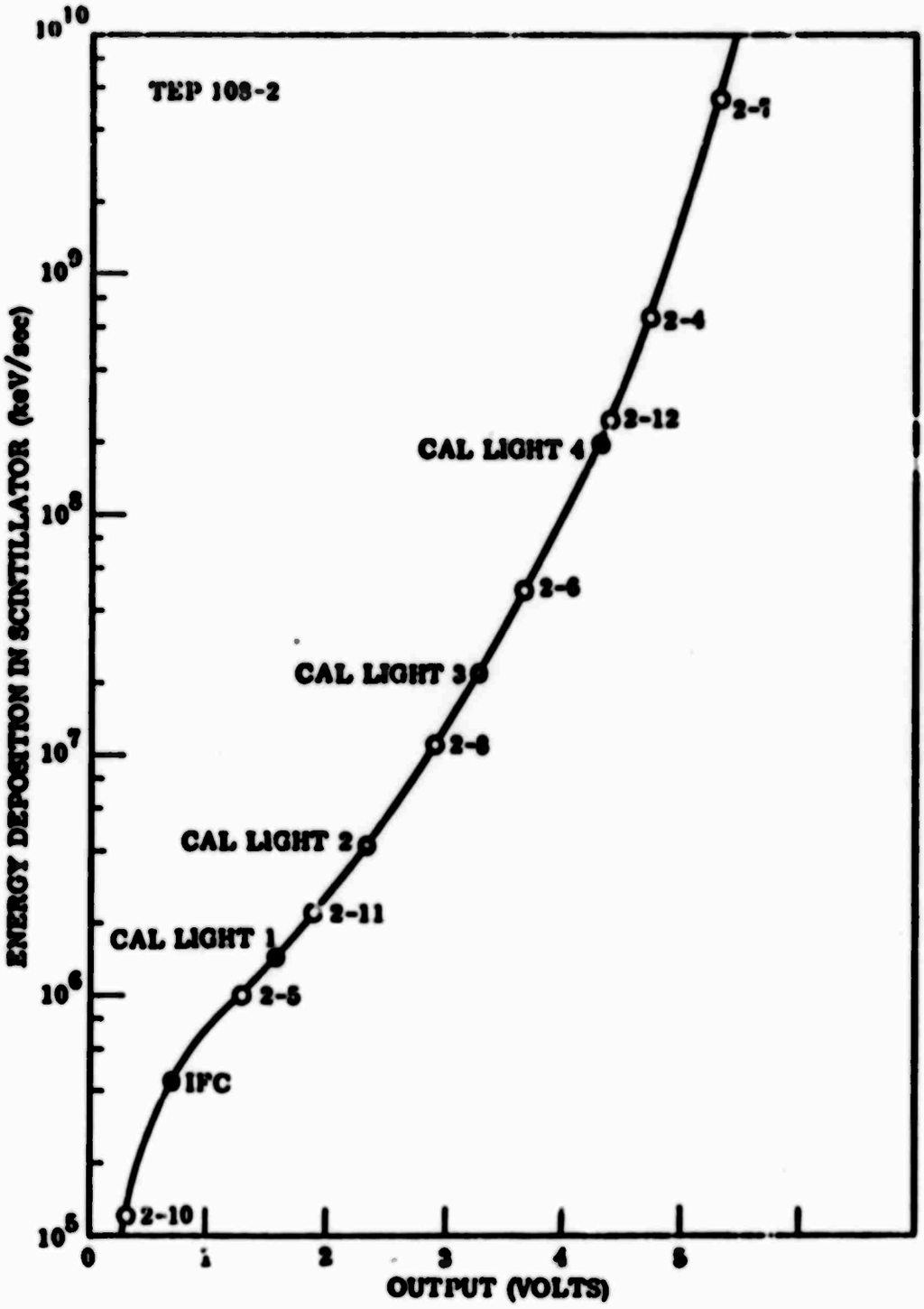

Figure 2.9 Calibration curve for TEP-2.

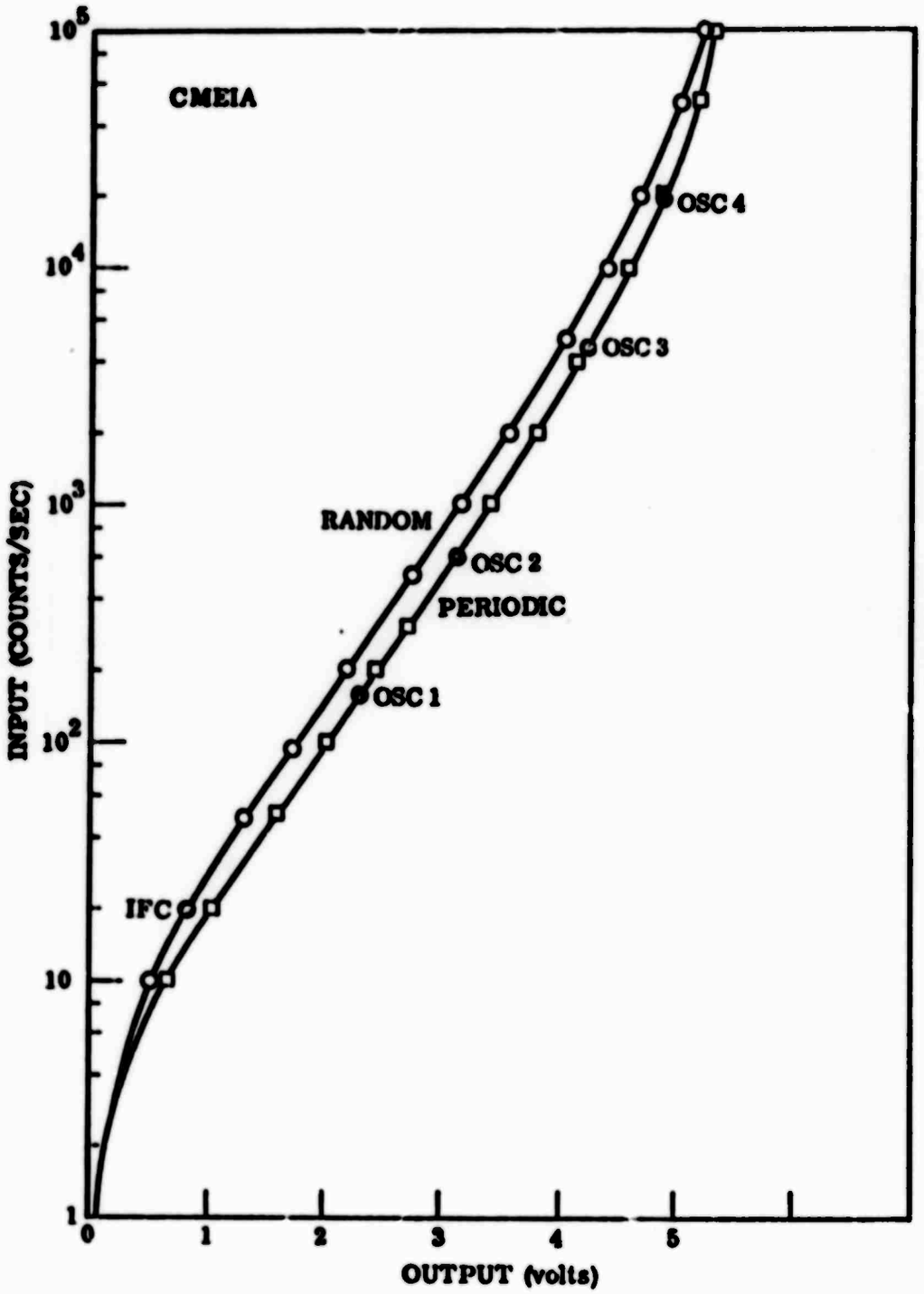

Figure 2.10 Calibration curve for CME-1A.

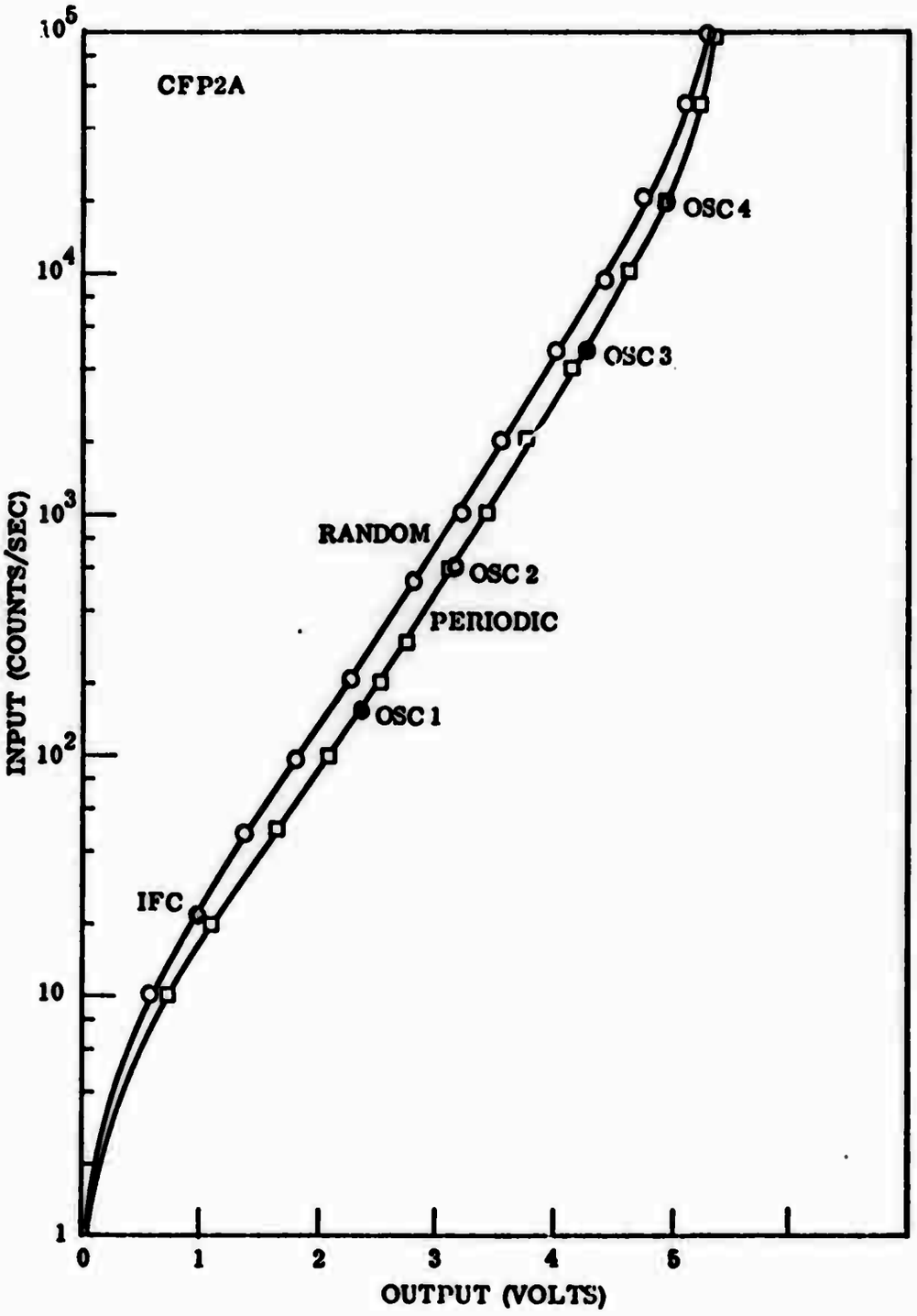

Figure 2.11 Calibration curve for CFP-2A.

periodic (sinusoidal) and one for random inputs. Included on the periodic curves are the points from the in-flight calibration oscillator which is used to calibrate all the ratemeters periodically during the course of the experiment. Also shown is the point from the in-flight radioactive calibration source which is included in each channel to indicate any possible changes in CEM counting efficiency during the course of the experiment. The measured responses of all of the various detectors at each step of the four-step calibration sequence and to their radioactive in-flight calibration sources are shown in Table 2-III. The laboratory measured values are shown as well as measurements taken in orbit both shortly after launch and after about a year's operation of the experiment. The overwhelming majority of the sensors were still functioning satisfactorily at that time.

In order to adequately measure the more penetrating particles found in the radiation belts and polar cap regions which can be a significant source of background to the low-energy detectors, an instrument called the PRM (Penetrating Radiation Monitor) has been included in the payload. This instrument possesses high-sensitivity and high-time resolution for the measurement of protons, electrons and alpha particles. Detection of protons in the energy range 1.2-46 MeV and integral above 70 MeV, electrons in the range 0.4-1.9 MeV and alpha particles in the range 7-20 MeV is performed with sensitivities as high as 0.1 particles/cm^2-sec and with a dynamic intensity range of six decades. The instrument employs a transmission solid-state detector having a total-depletion depth of 212 μm and a sensitive area of 300 mm^2 in conjunction with a total-energy plastic-scintillation spectrometer. The plastic-scintillator has a diameter of 6.5 cm and a thickness of 2.8 cm, corresponding to the range of a 58-MeV proton. Both detectors are surrounded with a minimum shielding of 5.0 gm/cm^2 corresponding to the range of a 60-MeV proton. A 1-mg/cm^2-thick mylar window, evaporated on both sides with 100-$\mu g/cm^2$ aluminum is placed across the entrance aperture to make the assembly light-tight and to prevent low-energy electrons and protons from entering the solid-state detector. The maximum acceptance half-angle of the aperture is 50 degrees and the omni-directional geometric factor for an isotropic flux is approximately 0.5 cm^2.

Table 2-III. LOW-ENERGY PARTICLE DETECTORS. IN-FLIGHT CALIBRATION RESULTS. (Sheet 1 of 4)

Detector Mode	Lab Test (1-24-69)	Flight Test (3-24-69)	Flight Test (4-20-70)	Detector Mode	Lab Test (1-24-69)	Flight Test (3-24-69)	Flight Test (4-20-70)
CFP-1B				CME-1F			
OSC-1	2.33	2.32	2.25	OSC-1	2.37	--	2.15
OSC-2	3.15	3.15	3.00	OSC-2	3.18	--	3.00
OSC-3	4.28	4.25	4.15	OSC-3	4.30	--	4.05
OSC-4	4.95	4.92	4.80	OSC-4	4.95	--	4.70
IFC Source	1.10	1.10	0.80	IFC Source	1.00	--	0.85
CFP-1D				CXA-1A			
OSC-1	2.24	2.24	2.10	OSC-1	1.81	1.85	1.80
OSC-2	3.05	3.03	2.95	OSC-2	2.72	2.77	2.70
OSC-3	4.14	4.09	4.00	OSC-3	3.90	3.95	3.88
OSC-4	4.76	4.76	4.65	OSC-4	4.70	4.70	4.65
IFC Source	0.90	0.95	0.80	IFC Source ON	0.20	--	0.10
				OFF	0.20	--	0.20
CME-1A				CXA-1B			
OSC-1	2.32	2.28	2.20	OSC-1	1.74	1.85	1.72
OSC-2	3.16	3.15	3.05	OSC-2	2.65	2.70	2.65
OSC-3	4.25	4.21	4.10	OSC-3	3.90	3.95	3.88
OSC-4	4.90	4.88	4.80	OSC-4	4.72	4.70	4.60
IFC Source	1.00	1.00	1.00	IFC Source ON	0.20	--	0.10
				OFF	0.60	--	0.25
CME-1B				CXA-1C			
OSC-1	2.31	2.28	2.20	OSC-1	1.80	1.80	1.75
OSC-2	3.12	3.11	3.00	OSC-2	2.70	2.70	2.62
OSC-3	4.21	4.17	4.00	OSC-3	3.90	3.85	3.75
OSC-4	4.85	4.84	4.70	OSC-4	4.65	4.70	4.50
IFC Source	1.10	1.10	0.75	IFC Source ON	0.20	--	0.10
				OFF	0.70	--	0.15
CME-1C				ADI-1			
OSC-1	2.25	2.24	2.15	Light 1	1.85	1.54	0.97
OSC-2	3.06	3.03	3.00	Light 2	2.42	2.09	1.62
OSC-3	4.15	4.13	4.05	Light 3	3.24	2.91	2.62
OSC-4	4.79	4.76	4.75	Light 4	4.10	3.90	3.60
IFC Source	1.00	0.95	0.80	IFC Source 1	1.09	0.95	0.50
				IFC Source 2	1.22	1.00	0.60
CME-1D				CMP-3A			
OSC-1	2.25	2.24	2.10	OSC-1	2.28	2.24	2.20
OSC-2	3.03	2.99	2.95	OSC-2	3.10	3.07	3.00
OSC-3	4.12	4.09	4.00	OSC-3	4.23	4.17	4.15
OSC-4	4.77	4.76	4.70	OSC-4	4.86	4.84	4.80
IFC Source	1.00	0.95	0.05	IFC Source	0.80	0.90	0.70
CME-1E				CMP-3B			
OSC-1	2.34	3.32	2.20	OSC-1	2.28	2.24	2.18
OSC-2	3.14	3.11	3.00	OSC-2	3.07	3.03	3.00
OSC-3	4.22	4.21	4.00	OSC-3	4.18	4.13	4.05
OSC-4	4.88	4.88	4.70	CSC-4	4.83	4.80	4.72
IFC Source	1.00	1.00	0.30	IFC Source	0.90	1.00	0.80

Table 2-III. LOW-ENERGY PARTICLE DETECTORS. IN-FLIGHT CALIBRATION RESULTS. (Sheet 2 of 4)

Detector Mode	Lab Test (1-24-69)	Flight Test (3-24-69)	Flight Test (4-20-70)	Detector Mode	Lab Test (1-24-69)	Flight Test (3-24-69)	Flight Test (4-20-70)
CMP-3C				CME-3B			
OSC-1	2.32	2.28	2.15	OSC-1	2.19	2.17	2.10
OSC-2	3.09	3.03	2.98	OSC-2	3.02	2.99	2.95
OSC-3	4.17	4.13	4.00	OSC-3	4.10	4.06	4.00
OSC-4	4.82	4.80	4.70	OSC-4	4.72	4.69	4.60
IFC Source	1.00	1.40	1.20	IFC Source	0.90	0.90	0.75
CFP-2A				CME-3C			
OSC-1	2.38	2.36	2.30	OSC-1	2.28	2.24	2.15
OSC-2	3.17	3.15	3.05	OSC-2	3.09	3.07	3.00
OSC-3	4.27	4.25	4.12	OSC-3	4.18	4.13	4.05
OSC-4	4.93	4.92	4.80	OSC-4	4.84	4.80	4.75
IFC Source	1.20	1.20	0.95	IFC Source	1.00	1.00	0.80
CFP-3B				CME-2D			
OSC-1	2.28	2.24	2.15	OSC-1	2.29	2.28	2.25
OSC-2	3.11	3.07	3.00	OSC-2	3.09	3.07	3.05
OSC-3	4.24	4.21	4.10	OSC-3	4.20	4.17	4.15
OSC-4	4.90	4.88	4.75	OSC-4	4.86	4.84	4.78
IFC Source	1.00	0.95	0.80	IFC Source	1.10	1.00	0.70
CFP-2C				CZU-2			
OSC-1	2.35	2.32	2.25	OSC-1	2.25	2.24	2.15
OSC-2	3.16	3.15	3.05	OSC-2	3.04	2.99	2.95
OSC-3	4.28	4.25	4.18	OSC-3	4.14	4.09	4.00
OSC-4	4.93	4.92	4.85	OSC-4	4.79	4.76	4.70
IFC Source	1.20	1.15	0.90	IFC Source	1.30	1.80	0.35
CFP-3D				ADI-2			
OSC-1	2.30	2.28	2.10	Light 1	1.30	1.65	1.22
OSC-2	3.09	3.07	2.90	Light 2	1.90	2.01	1.88
OSC-3	4.20	4.13	4.00	Light 3	2.70	2.76	2.76
OSC-4	4.87	4.84	4.68	Light 4	3.90	3.78	3.80
IFC Source	1.20	1.20	1.05	IFC Source 1	0.80	--	0.65
				IFC Source 2	0.90	--	0.75
CFP-2E				TEP-108-1			
OSC-1	2.30	--	2.15	Light 1	1.63	1.50	1.62
OSC-2	3.09	--	3.05	Light 2	2.35	2.24	2.40
OSC-3	4.13	--	4.00	Light 3	3.14	3.11	3.22
OSC-4	4.80	--	4.70	Light 4	4.09	4.13	4.18
IFC Source	1.30	--	1.00	IFC Source	0.68	0.55	0.50
CME-2A				TEP-108-2			
OSC-1	2.30	2.28	2.20	Light 1	1.51	1.97	0.75
OSC-2	3.11	3.07	3.00	Light 2	2.29	2.28	1.60
OSC-3	4.22	4.17	4.10	Light 3	3.24	3.11	2.68
OSC-4	4.86	4.84	4.75	Light 4	4.21	4.09	3.30
IFC Source	1.00	1.00	0.70	IFC Source	0.93	0.50	0.35

Table 2-III. LOW-ENERGY PARTICLE DETECTORS. IN-FLIGHT CALIBRATION RESULTS. (Sheet 3 of 4)

Detector Mode	Lab Test (1-24-69)	Flight Test (3-24-69)	Flight Test (4-20-70)	Detector Mode	Lab Test (1-24-69)	Flight Test (3-24-69)	Flight Test (4-20-70)
CFP-4B				CFE-4B			
OSC-1	2.31	2.28	2.20	OSC-1	2.34	2.32	2.25
OSC-2	3.13	3.11	3.05	OSC-2	3.13	3.11	3.05
OSC-3	4.26	4.21	4.10	OSC-3	4.22	4.17	4.10
OSC-4	4.92	4.88	4.75	OSC-4	4.88	4.84	4.75
IFC Source	1.20	1.30	1.10	IFC Source	1.50	1.50	1.20
CFP-4D				CFE-4C			
OSC-1	2.38	2.32	--	OSC-1	2.25	2.20	2.10
OSC-2	3.18	3.15	--	OSC-2	3.05	3.03	2.88
OSC-3	4.26	4.21	--	OSC-3	4.18	4.13	3.95
OSC-4	4.92	4.88	--	OSC-4	4.83	4.80	4.65
IFC Source	1.10	1.20	--	IFC Source	1.20	1.10	0.90
CME-4A				ADI-3			
OSC-1	2.36	2.32	2.27	Light 1	1.10	1.73	0.90
OSC-2	3.18	3.15	3.10	Light 2	1.50	2.20	1.57
OSC-3	4.29	4.25	4.20	Light 3	2.50	3.07	2.49
OSC-4	4.94	4.92	4.90	Light 4	3.50	3.94	3.49
IFC Source	1.00	1.00	0.75	IFC Source 1	0.80	0.91	0.45
				IFC Source 2	0.90	1.06	0.55
CME-4B				CFP-5B			
OSC-1	2.33	2.28	2.25	OSC-1	2.37	2.36	--
OSC-2	3.14	3.11	3.10	OSC-2	3.18	3.15	--
OSC-3	4.25	4.21	4.20	OSC-3	4.28	4.25	--
OSC-4	4.88	4.84	4.90	OSC-4	4.94	4.92	--
IFC Source	0.90	1.00	0.80	IFC Source	1.20	1.30	--
CME-4C				CFP-5C			
OSC-1	2.35	2.32	2.25	OSC-1	2.34	2.24	2.10
OSC-2	3.17	3.15	3.05	OSC-2	3.18	3.07	2.92
OSC-3	4.27	4.25	4.15	OSC-3	4.29	4.17	3.95
OSC-4	4.90	4.88	4.75	OSC-4	4.97	4.84	4.70
IFC Source	1.20	0.90	0.80	IFC Source	1.00	0.95	0.20
CME-4D				CFP-5D			
OSC-1	2.33	2.28	2.10	OSC-1	1.00	2.32	--
OSC-2	3.15	3.11	3.05	OSC-2	2.34	3.15	--
OSC-3	4.29	4.21	4.10	OSC-3	3.18	4.25	--
OSC-4	4.91	4.88	4.80	OSC-4	4.29	4.92	--
IFC Source	0.80	0.90	0.65	IFC Source	4.97	1.00	--
CFE-4A				CFP-5E			
OSC-1	2.32	2.28	2.25	OSC-1	2.36	--	--
OSC-2	3.13	3.11	3.05	OSC-2	3.19	--	--
OSC-3	4.25	4.21	4.15	OSC-3	4.29	--	--
OSC-4	4.92	4.88	4.82	OSC-4	4.94	--	--
IFC Source	1.60	1.70	1.35	IFC Source	1.10	--	--

Table 2-III. LOW-ENERGY PARTICLE DETECTORS. IN-FLIGHT CALIBRATION RESULTS. (Sheet 4 of 4)

Detector Mode	Lab Test (1-24-69)	Flight Test (3-24-69)	Flight Test (4-20-70)
CME-5A			
OSC-1	2.34	2.32	--
OSC-2	3.13	3.11	--
OSC-3	4.23	4.21	--
OSC-4	4.89	4.88	--
IFC Source	1.40	1.40	--
CME-5B			
OSC-1	2.37	2.36	2.25
OSC-2	3.19	3.15	3.05
OSC-3	4.30	4.25	4.05
OSC-4	4.97	4.96	4.75
IFC Source	1.60	1.70	0.20
CME-5C			
OSC-1	2.32	2.28	2.25
OSC-2	3.13	3.11	3.05
OSC-3	4.25	4.21	4.15
OSC-4	4.91	4.88	4.82
IFC Source	1.70	1.60	1.15
CME-5D			
OSC-1	2.37	2.36	2.25
OSC-2	3.18	3.15	3.10
OSC-3	4.29	4.25	4.15
OSC-4	4.95	4.92	4.85
IFC Source	1.80	1.80	1.15
CZU-5			
OSC-1	2.36	2.36	--
OSC-2	3.19	3.19	--
OSC-3	4.31	4.29	--
OSC-4	4.96	4.92	--
IFC Source	1.30	--	1.10
CFE-5			
OSC-1	2.30	--	2.30
OSC-2	3.09	--	3.09
OSC-3	4.22	--	4.05
OSC-4	4.88	--	4.75
IFC Source	1.50	--	0.05

Acceptable pulses from each detector, as determined by various combinations of coincidence logic, are analyzed with separate 15-channel pulse-height analyzers of the analog-to-digital type.

Section 2

REFERENCES

1. Harris, K. K., G. W. Sharp and W. C. Knudsen, "Ion temperature and relative ion composition measurements from a low-altitude polar-orbiting satellite," J. Geophys. Res., 72, 5939 (1967).

2. Nagy, A. F., and A. Z Faruqui, "Ionospheric electron density and body potential measurements by a cylindrical Langmuir probe," J. Geophys. Res., 70, 4847 (1965).

3. Reagan, J. B., D. L. Carr, J. D. McDaniel and L. F. Smith, "Satellite instrumentation for the measurement of auroral phenomena," IEEE Trans. Nucl. Sci., NS-11, No. 3, 441 (1964).

4. Reagan, J. B., D. L. Carr, J. D. McDaniel and T. C. Sanders, "Low-energy electron and proton satellite instrumentation for auroral studies," IEEE Trans. Nucl. Sci., NS-14, No. 1, 49-55 (1967).

5. Shea, M. F., G. B. Shook, J. B. Reagan, L. F. Smith and T. C. Sanders, "Channel multiplier instrumentation for the measurement of low-energy auroral particles," IEEE Trans. Nucl. Sci., NS-14, No. 1, 96-102 (1967).

BLANK PAGE

Section 3

OPERATIONS

3.1 Satellite Performance

Between 18 March 1969 and 28 April 1970, the OV1-18 satellite has completed 6161 orbits in space. Of this total number, there have been 658 telemetry acquisitions of the satellite by the eight tracking stations in the net. During 611 of these acquisitions, tape-recorded data were transmitted to the station at a 16:1 reproduce/record ratio. In this manner, slightly greater than one complete orbit of data (100 minutes) were obtained for each station pass. The remaining data consists of real-time passes over a station, particularly over the Ascension Island tracking station which is located in the South Atlantic anomaly region.

Analog telemetry tapes recorded at the respective tracking stations were shipped to Cape Kennedy where they were dubbed and used to generate a computer-compatible, digital-formatted tape. Both the analog and digital tapes for each pass were made available to the various experimenters. Upon receipt, all analog tapes were surveyed at the Lockheed Research Laboratory Data Processing facility. Key experiment data and satellite status data were immediately processed on 12-channel pen recorders. A log of satellite performance parameters including transmitter signal strength, tape recorder data quality, solar cell-battery power output, temperature, command responses, and orientation in the geomagnetic field was accurately maintained. In general, with the one exception of satellite orientation stability, the overall performance of the OV1-18 spacecraft can be described as excellent.

Evaluation of the satellite power system indicates that the solar cells have provided and are providing sufficient voltage and current to the vehicle regulator to maintain the experiment power bus at an extremely stable +28 $\pm$ 0.04 VDC. Analysis of several temperature monitors throughout the 14-month period of operation has revealed an experiment operating range from +18°C to +25°C, a remarkedly narrow and desired range.

Telemetry signal strength from the satellite has been sufficiently high such that excellent signal-to-noise ratios have been consistently achieved. On many acquisitions, it is not unusual to process a complete 100 minutes of tape-recorded data containing over 10^7 bits of data without the loss of a single bit. The average bit-error rate has been approximately one part in 10^5 which still results in high-quality data. An apparent variation in tape recorder speed was observed during May 1969, but this problem corrected itself and normal performance has been observed since that time.

As a result of difficulties in deploying the gravity-gradient stabilization booms shortly after launch, the OV1-18 satellite never achieved the desired three-axis, earth-centered stabilization. Initially, the satellite instability manifested itself as a relatively slow tumble with a rate of 0.01 per minute or approximately one complete revolution per orbit. The tumble rate slowly increased in an approximately linear manner to 0.28 revolutions per minute as shown in Figure 3.1 until mid-September 1969 when one or more of the booms apparently came free of the satellite. At this point, the tumble rate increased more dramatically to a maximum value of 0.48 revolution per minute and then slowly decreased to the present value of approximately 0.40 revolution per minute. The tumble rate was continuously monitored along the three principle vehicle axes by a tri-axis magnetometer. As discussed in the data analysis section, a detailed analysis of these magnetometer outputs revealed that residual offsets existed. A correction program was incorporated into the data processing loop to compensate for these offsets. The resultant instrument and satellite orientation data with respect to the geomagnetic field is thought to be accurate to a few degrees. The most significant effect that the lack of vehicle stability has produced is a reduction in the fraction of time spent observing desired phenomena, for example, the instruments are oriented toward the earth during an appreciable portion of an orbit. However, since each instrument orientation in the geomagnetic field is known at all times, valuable information is obtained when the orientation is favorable.

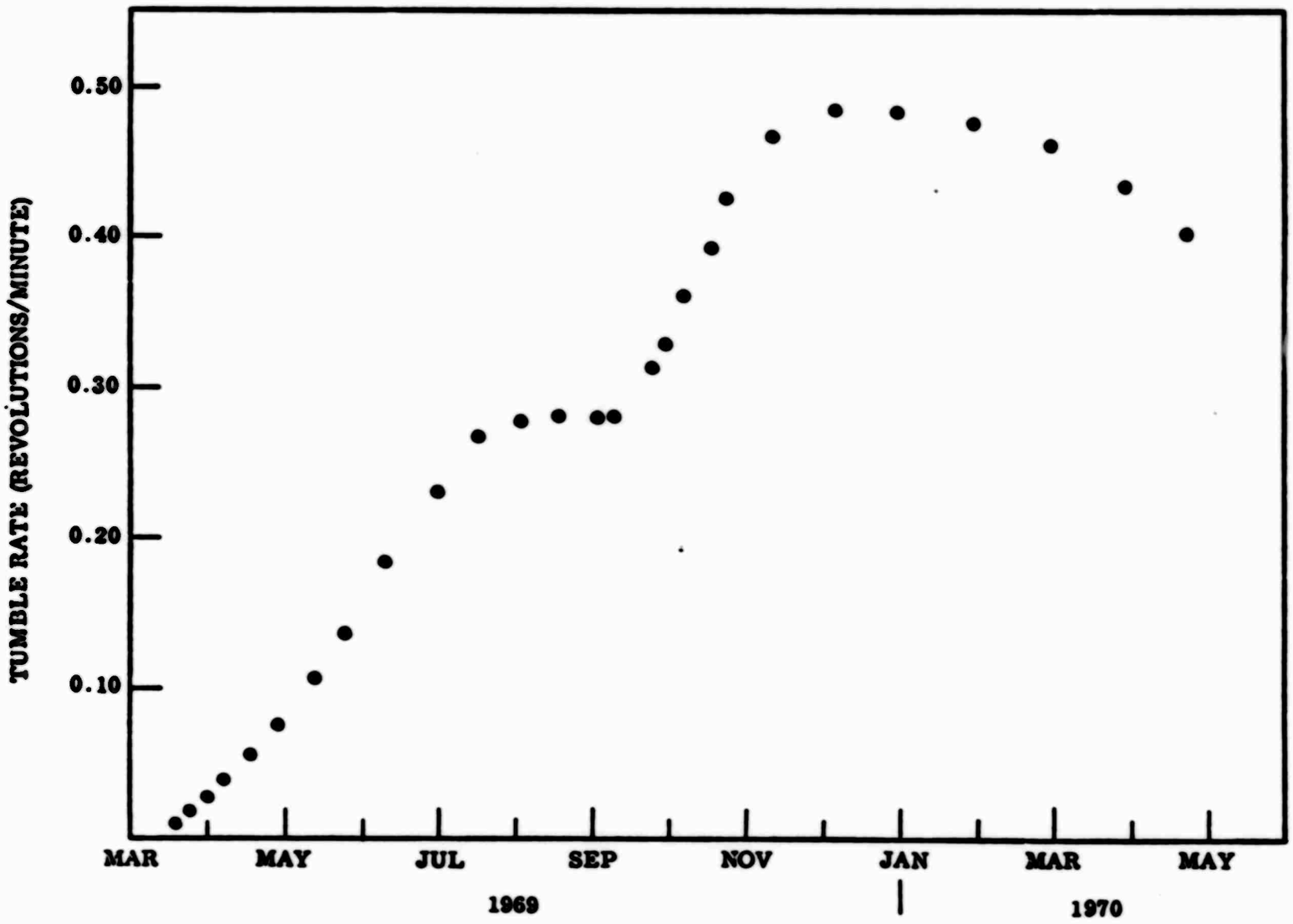

Figure 3.1 Tumble rate of satellite during the course of the experiment.

Table 3-I contains a summary of the data acquired from the OV1-18 satellite along with the number of analog tapes which have been surveyed for key data. Complete analog pen recordings of all the experimental data have been processed from 52 tape-recorded passes. In addition, 86 tape-recorded orbits have been processed through the Lockheed UNIVAC-1108 digital computer. This latter process utilizes the formatted digital tapes mentioned earlier and allows detailed scientific calculations to be performed on the data. The various software programs which were developed under this contract to process these data are described in the data analysis section.

Table 3-I Extent of Data.

1.	Satellite orbits (18 March 1969 - 28 April 1970)		6161
2.	Data acquisitions		658
	a. Tape recorded orbits	611	
	b. Real-time station passes	47	
3.	Processed data		
	a. Analog survey pen recordings		562
	1. 36 tapes not received		
	2. 13 tapes too noisy for processing		
	b. Analog pen recordings for all experiment data		52
	c. Digital tapes processed through UNIVAC-1108 computer		86

3.2 Instrument Performance

The overwhelming majority of the instruments in the payload performed well and are still producing useful data over a year after launch. All twelve of the particle instruments functioned as designed and are still operating although some of the specially designed channel-electron-multipliers in one instrument (the Electric Field Probe or EFP) have experienced gain fatigue and are no longer producing useful data. These multipliers require a longer outgassing period than the conventional units and several of them suffered a period of corona discharge when the satellite payload was turned on earlier than expected on orbit 51. This early turn-on

was decided upon because persistent drops in the telemetry power output during the first three days caused some concern about the possible early failure of the telemetry. The problem later cleared itself up, however, and as has been indicated, the telemetry functioned well for the remainder of the experiment.

The ion energy analyzer worked well for a period of 225 orbits. All experiment monitors indicate normal instrument operation over this period. As has been indicated, the two-axes stabilization of the vehicle was not achieved and thus the programmed operation of the IEA was not as effective as had been planned; however, the data may be retrieved by appropriate analysis. A sample of the data thus obtained is shown in Figure 3.2. This data was obtained from just one sensor element and is typical of the data found from the other sensor elements. The data presented in Figure 3.2 is quick-look ion density data and has been processed by hand. No effort has yet been made to normalize this raw data to the velocity vector direction. The character of the data is, however, interesting in that it clearly shows that large horizontal gradients in the ion density do exist. The complete analysis of the data awaits, however, the determination of the attitude of the vehicle as a function of orbit position.

Although not uniquely determined, the failure of the instrument may have resulted from the required addition of the three extra sensor elements. The four sensor elements, when operated together, required operation nearer to the output limit of the instrument power supply than with one sensor. Short-term tests and circuit analysis showed the performance to be satisfactory, but the constraints of time imposed by the launch schedule precluded long-term tests.

The cylindrical Langmuir probe operated as designed from instrument turn-on to the present time. Selected orbits of data have been analyzed by hand. Complete analysis of the data awaits the orbit-attitude information. An example of an actual data record is shown in Figure 3.3 in which one complete data cycle is given. The upper trace corresponds to the potential applied to the probe. The lower trace represents the data output from which the characteristic volt-ampere curves are constructed. The

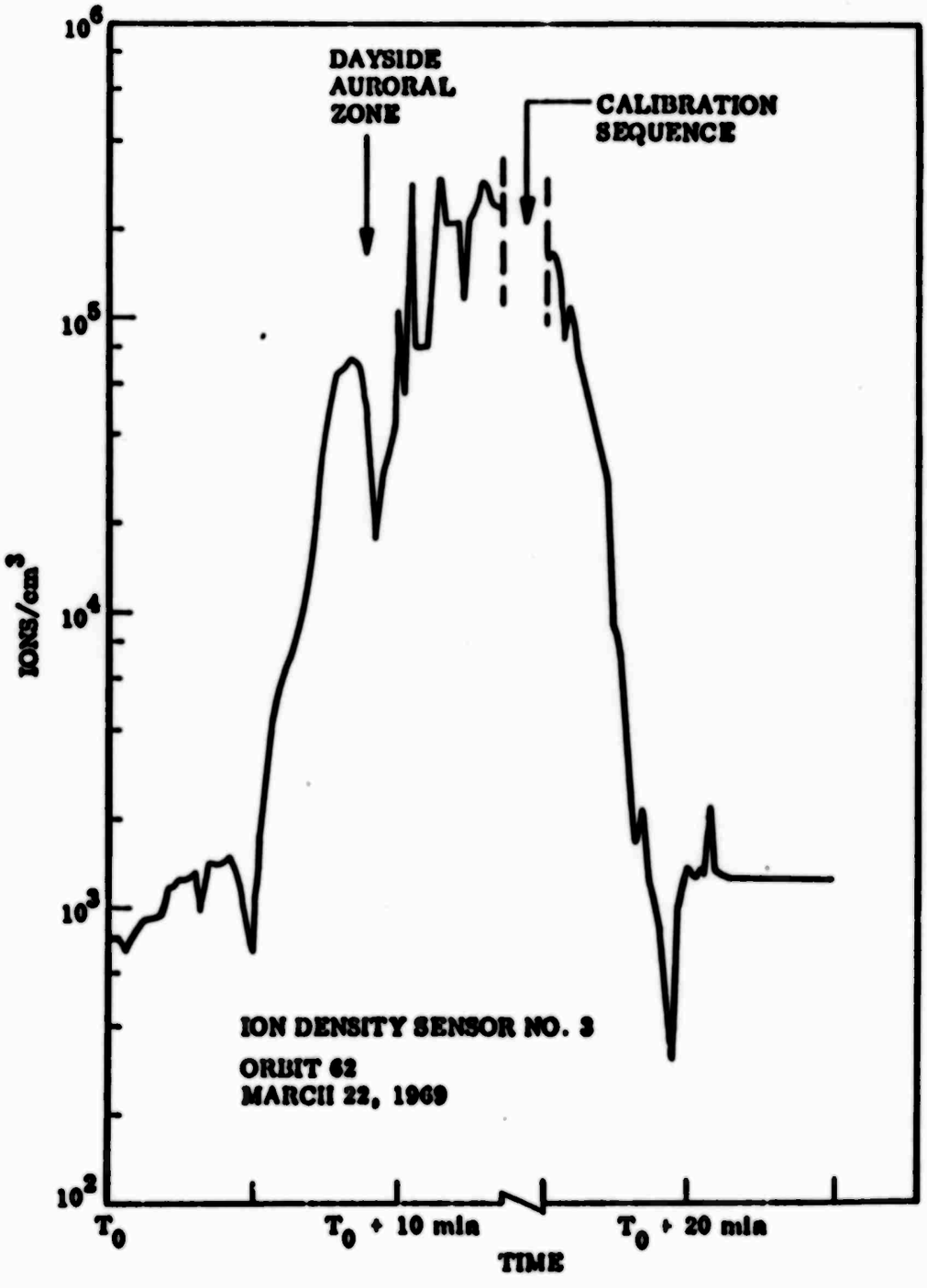

Figure 3.2 Sample data from Ion Energy Analyzer.

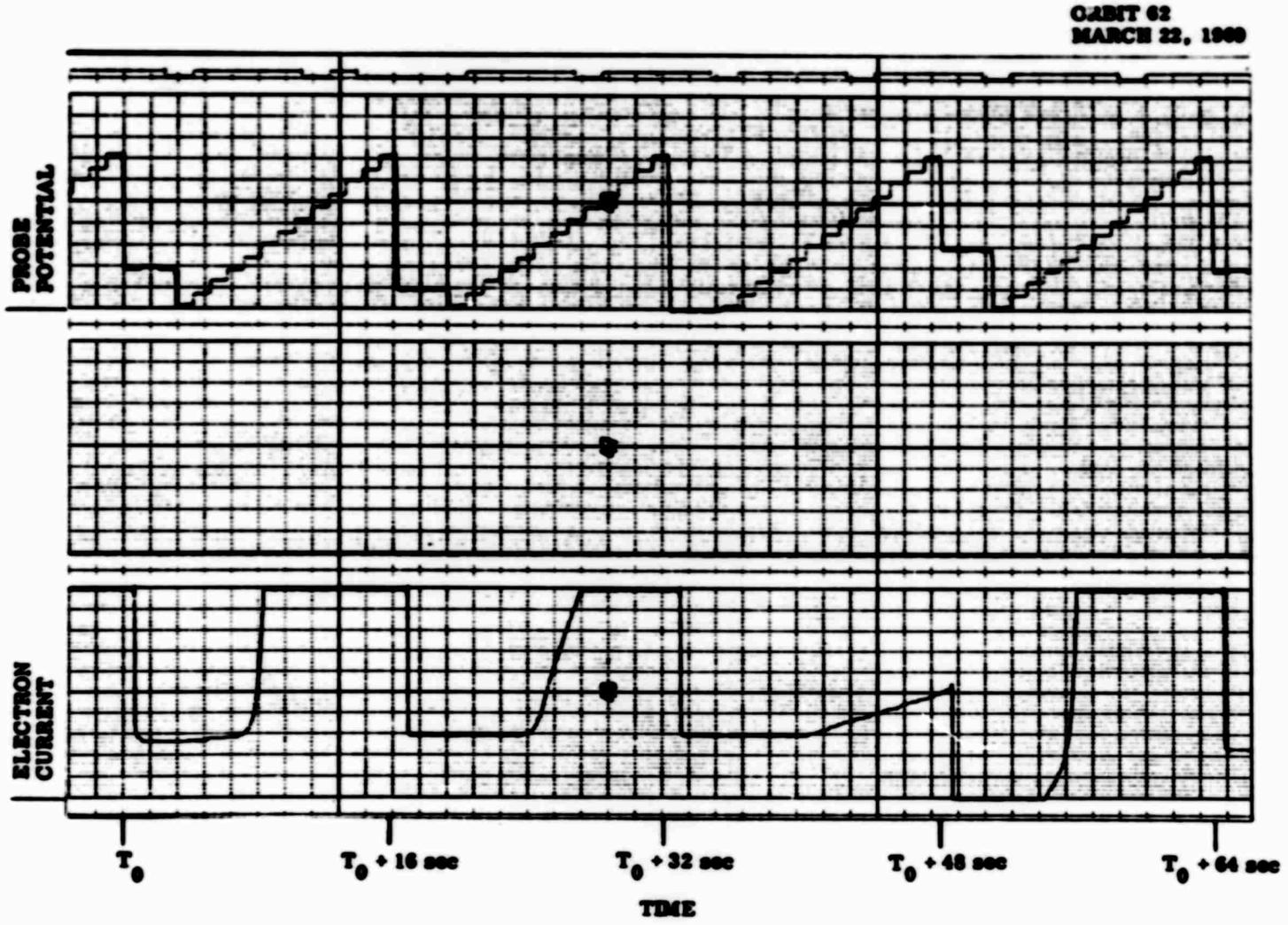

Figure 3.3 Sample data from Langmuir probe.

electron temperature and density are subsequently obtained from the analysis of the volt-ampere curves.

The EEA experiment operated as designed for approximately one and one-half orbits of data acquisition. Samples of telemetry output for the three sensor heads over several instrument cycles and during the first orbit of data acquisition is illustrated in Figure 3.4. The top signal, labeled Phase, indicates the retarding potential applied to the retarding grid and also the high and low current calibration phases. The other three signals indicate the telemetry voltage corresponding to the electron current collected by each sensor. Only a few individual cycles have been analyzed, two of which will be presented in Figure 4.10 in the data analysis section. During the second orbit of data acquisition, the instrument failed from an undetermined cause. However, the uniqueness of this low-energy electron data makes only one and a half orbits of data of significant value.

3.3 Coordinated Observations

For selected periods, the satellite experiment has also provided quantitative measurements of the particle flux inputs to the ionosphere for intercomparison with coordinated ground-based observations of various ionospheric phenomena. Of particular interest is a study of the relationship between radar clutter and refraction phenomena and the auroral particle fluxes. Three sets of coordinated satellite and ground-based radar observations have been carried out, two in cooperation with the radar group at Stanford Research Institute utilizing their facility at Homer, Alaska, and one with the radar group at the MIT Lincoln Laboratory (ABMDA). The first set of coordinated measurements were obtained over a six-week period between 23 March and 8 May 1969 during twenty-seven traversals of the satellite over the Fairbanks area. Radar auroras were observed on most of the passes and preliminary scans of the satellite data from 24 passes has shown that particle precipitations were occurring on each of the overpasses when radar returns were reported. The second set of coordinated measurements was made during a seven-week period between 1 September and 17 October 1969 during thirty-one traversals of the satellite over the Fairbanks area. For the experiment with the MIT Lincoln

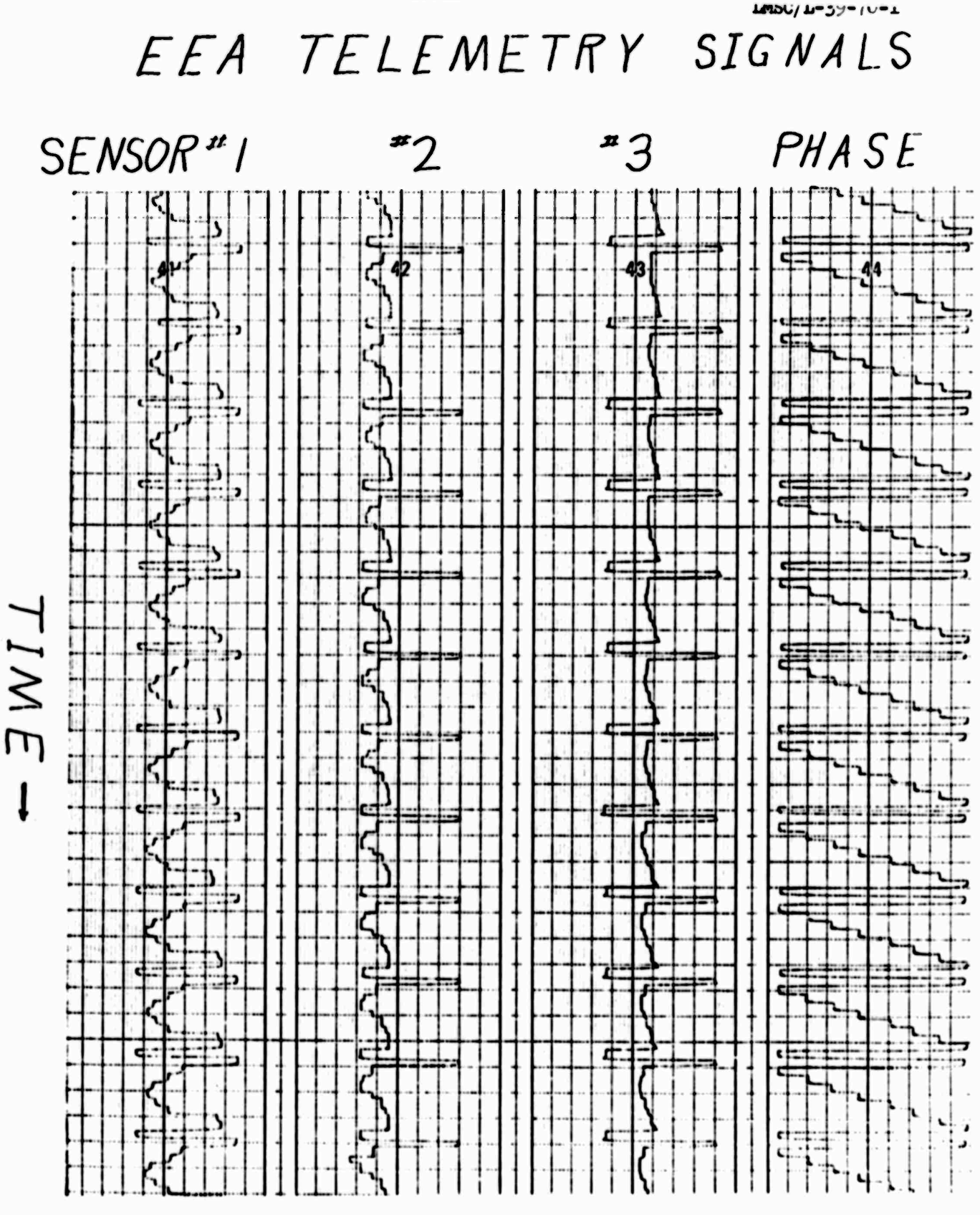

Figure 3.4 Sample data from epithermal electron analyzer.

Laboratory, the satellite was operated for thirteen dayside passes over Quebec Province in Canada during the period 10 April to 17 April 1970.

A set of coordinated measurements was also obtained with the DASA PCA-69 operation at Fort Churchill, Canada, during which the satellite provided measurements on the solar particle event which was in progress at the time, and determined the contributions to the disturbed ionosphere made by the low-energy (auroral) particles at the times of the overpasses. During this period (2-5 March 1969) the satellite was programmed to obtain seven overpasses of the Churchill area and large fluxes of solar protons in the 1 to 10-MeV range as well as energetic solar electrons and alpha particles and auroral particles were observed.

The satellite was also specially programmed during the period of 24 November to 18 December 1969 for coordinated observations with the NASA 1969 Airborne Auroral Expedition and simultaneous data were obtained on auroral precipitation events.

Section 4

PRELIMINARY DATA ANALYSIS

Several complementary techniques have been utilized to process and to assess the data as it has been received. For each acquisition, one or more survey plots showing the outputs of some representative detectors has been made from the analog tape by means of the Lockheed ground station which decodes and demultiplexes the signal and produces an analog strip chart containing six selected instrument outputs. Since this process is entirely analog, the digital time base information from the satellite is not readily available and so the plots have an unnormalized time scale. They are extremely useful, however, to indicate the quality of the data, to verify that the payload is still functioning normally, and to give a rough indication of the general level of particle fluxes.

Figure 4.1 shows the raw data from several representative detectors in this survey format. Relative time is plotted along the horizontal axis. The period shown corresponds to one complete tape recorder dump (100 minutes) or somewhat more than one orbit. The upper curve shows the output of the CME-1A in the range from 0 to 5 volts. This detector responds to electrons with energies between 0.8 and 1.5 keV. The two spikes shortly after turn-on are an in-flight calibration sequence. The satellite at this point is heading south on the nightside of the earth toward the auroral zone. An enhanced flux is observed during the south polar crossing and the instrument returns to its background level (defined by the in-flight radioactive calibration source) as the satellite heads north on the dayside. The large noise spike in the center of the record is from the reversal of the tape on the recorder. The satellite then crosses the northern auroral zone on the dayside, goes through the polar cap region where the flux goes down to background level and then crosses the auroral zone again on the nightside heading south. The two spikes are from another in-flight calibration sequence and the tape ends with a slight enhancement due to the penetrating particles in the radiation belt. The reason that the dayside and nightside auroral zones are merged in the southern hemisphere and separated in the north is that for this particular traversal the orbit reached higher magnetic latitudes in the north.

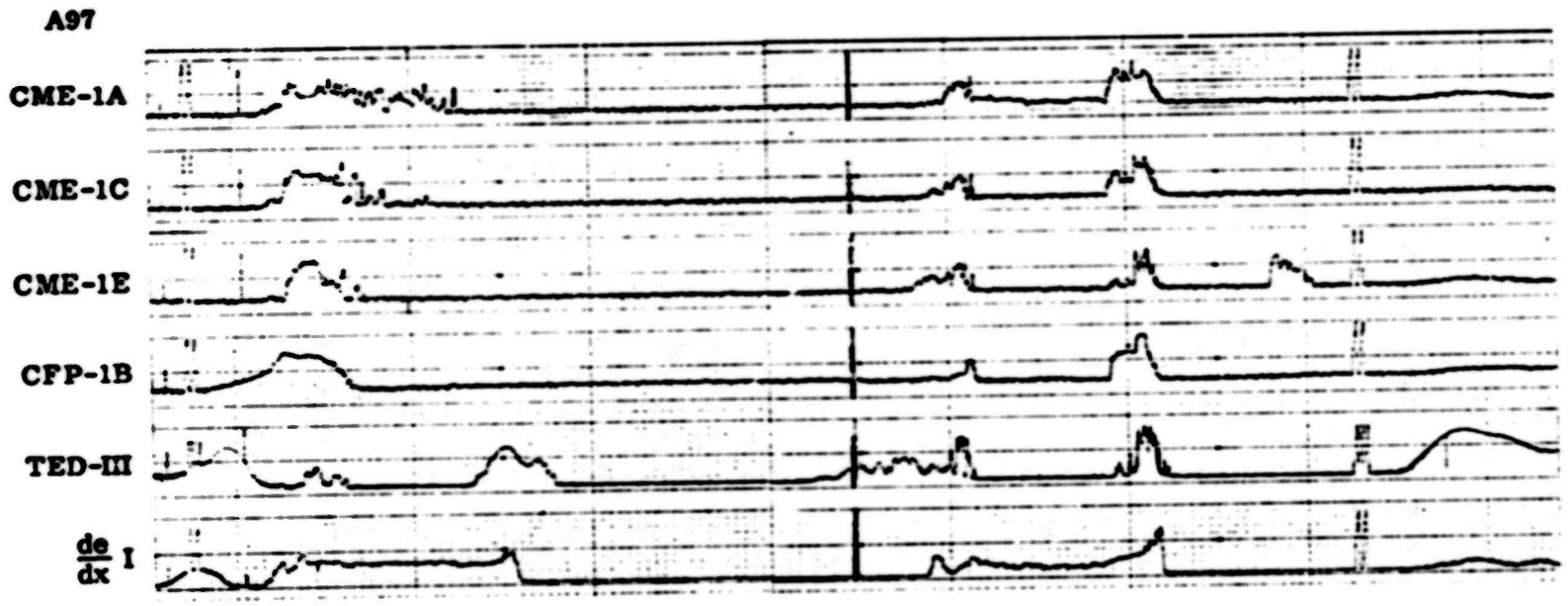

Figure 4.1 Sample data from six particle detectors in the survey format.

The next two curves show similar results for CME-1C (3.75 to 7.0 keV electrons) and CME-1E (17.3 to 37.0 keV electrons). The region of enhanced count rate in CME-1E just prior to the second calibration sequence is a spurious response. The fourth curve down shows the output of CFP-1B (protons with energies greater than 10 keV). All of these instruments used channel-electron-multipliers as the sensors. The bottom two curves show the outputs of two of the scintillator-photomultiplier detectors. The TED-3 response is proportional to the total energy flux of electrons with energies above about 25 keV. This response reaches a maximum at latitudes below the auroral zones in the region of the outer radiation belt. The lower curve shows the output of one of the channels of the Penetrating Radiation Monitor (PRM) which is sensitive to protons in the MeV range. A solar proton event was in progress during the period illustrated and the energetic protons were seen over both polar caps.

The next stage of analysis is performed by a computer program which processes the Air Force-supplied digital tapes for selected orbits and produces a complete set of survey plots showing the outputs of 50 detectors on six different strip charts with a normalized time base. The program first unpacks the digital tapes through a logical bit manipulation which converts the 48-bit words into 1108-compatible 36-bit words and then stores them on magnetic tape in a converted form for further processing. In order to plot this large quantity of data at a reasonable cost, it was necessary to make use of five drums for storage and to use a sleuth routine for changing the buffer size of the plot-output tape. A short section from each of three of the six strip charts are shown in Figures 4.2, 4.3 and 4.4 during a traversal of the northern polar region on 13 April 1970. The abscissa is a continuously running time index in seconds. The channels with a common pointing direction are grouped together and the top curve in each figure shows the pitch angle corresponding to this pointing direction as a function of time as computed from the on-board magnetometer data. The scale varies from 0° to 180° with 0° corresponding to particles coming down into the atmosphere in the southern hemisphere. The nominal 55° detectors are further subdivided into two groups. The pitch angle corresponding to the TEP detectors is shown in the light

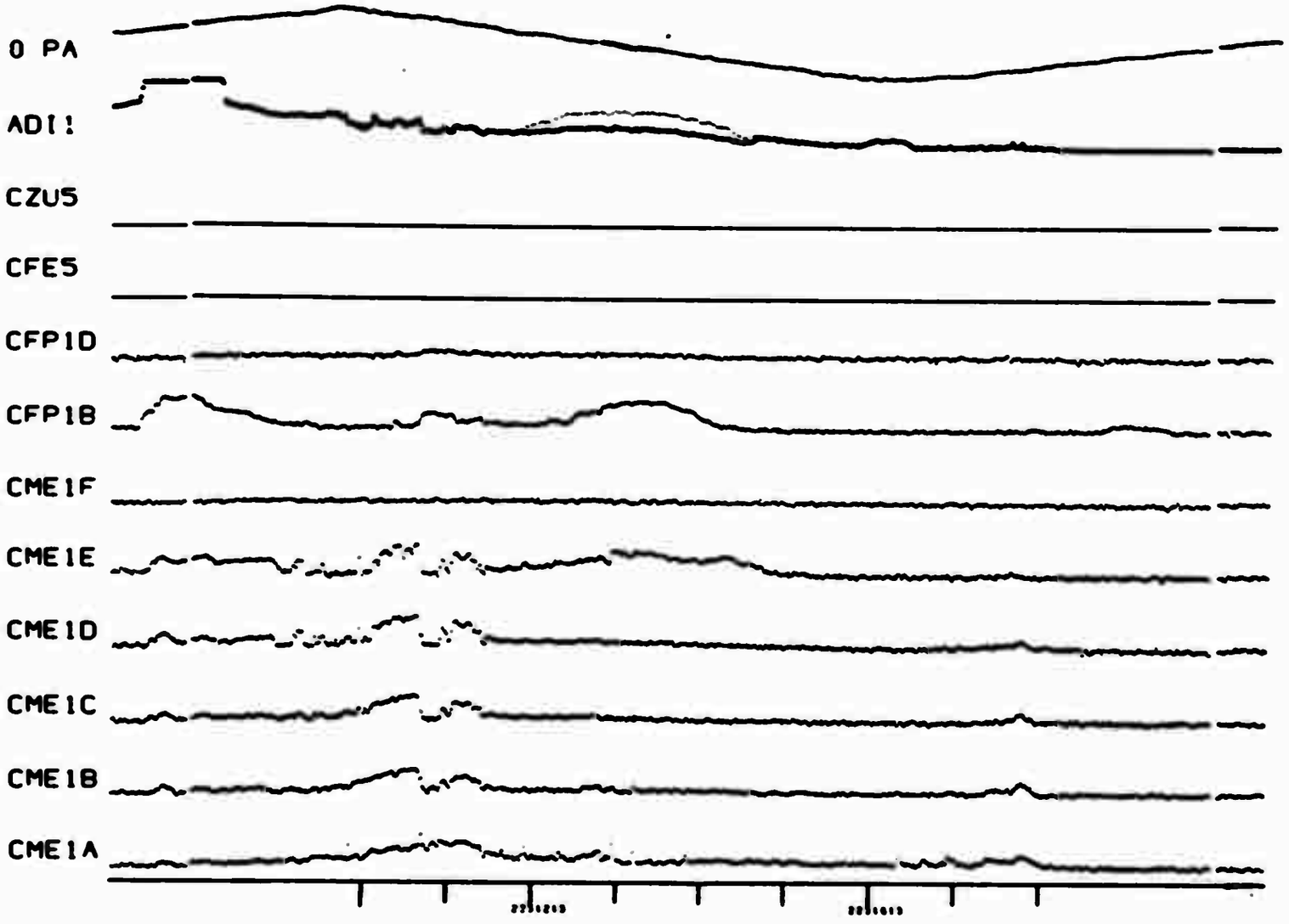

Figure 4.2 Particle data from the nominal 0° detectors during a traversal of the northern polar region on 13 April 1969.

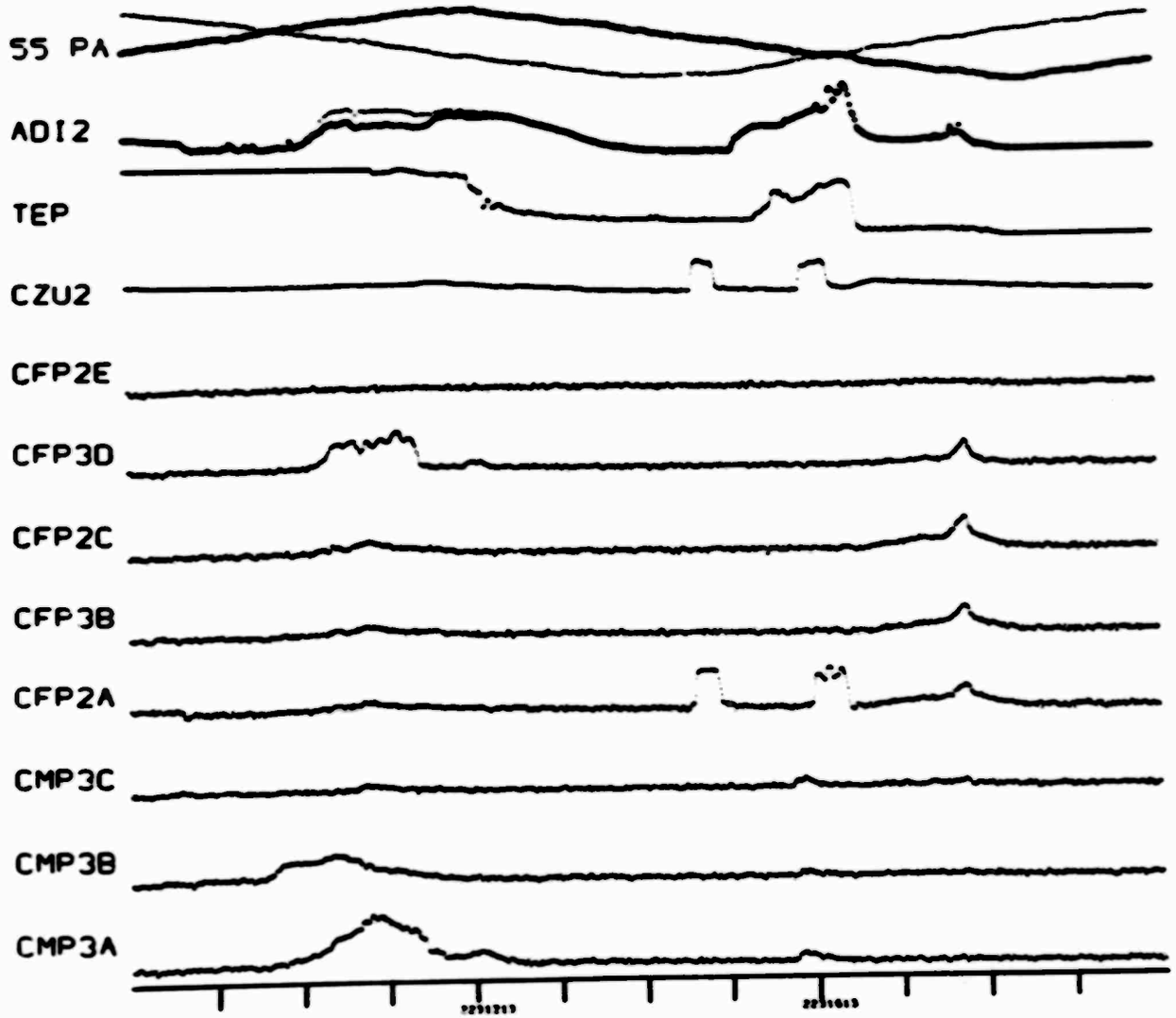

Figure 4.3 Particle data from the nominal 55° detectors during a traversal of the northern polar region on 13 April 1969.

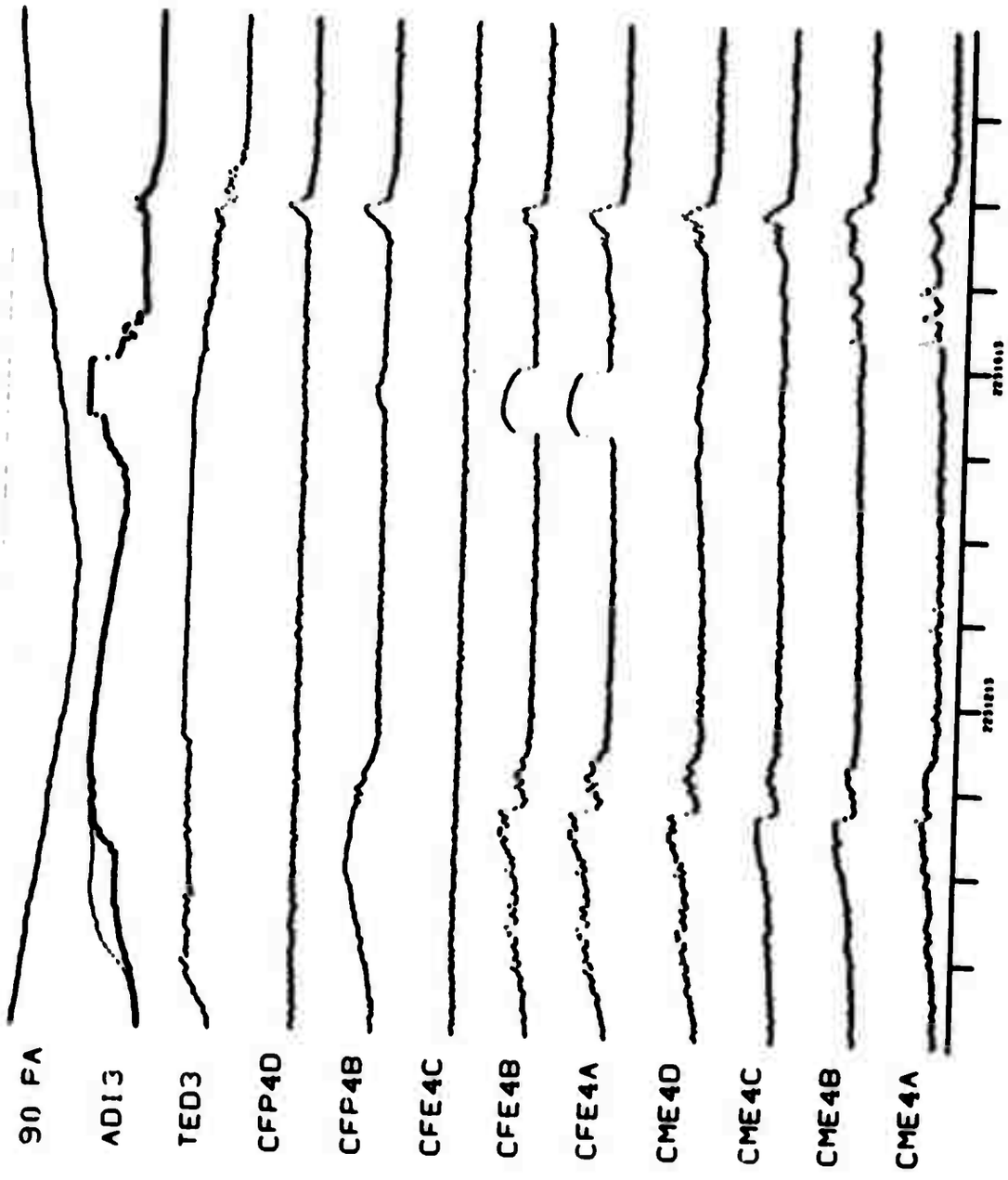

Figure 4.4 Particle data from the nominal 90° detectors during a traversal of the northern polar region on 13 April 1969.

curve while that for the remaining detectors is shown in the darker curve. Two curves are also shown for the ADI instruments. The light curve indicates the instrument response when on its 1.2-kilovolt threshold and the dark curve is the 0.2-kilovolt threshold response. Each of the other curves shows the output of an individual detector in the range 0 to 5 volts. The traversals of the dayside auroral zone at about 2231100 seconds and the nightside auroral zone at about 2231800 are marked by enhanced and fluctuating responses in both the electron and proton channels. Care must be exercized in interpreting these raw data since several varieties of spurious response are present. For example, in Figure 4.4, at about 2231550, the nominal 90^{o} detectors are looking at the sun as indicated by the saturated response of ADI-3 and the high smooth peaks in the CFE's. The peak at about 2231480 in the CFP-2A response in Figure 4.3 is due to ultraviolet light (Cf., the UV monitor CZU-2). The enhanced response at about 2231300 in CFP-1P and the enhanced response of ADI-1 in Figure 4.2 are due to the "scooping up" of plasma which occurs when these detectors are oriented in the velocity direction during the tumbling of the spacecraft. This type of record has been found invaluable in determining the regions and extent of spurious response and in selecting particularly interesting segments of data for detailed analysis.

A computer program to perform the next step in the detailed analysis of the precipitating fluxes for selected periods has also been developed. It uses as input the 1108 compatible magnetic tape produced by the above-described program and also the calibration curves, geometric factors, energy ranges and background levels of the various channels. The responses of thirty-one detectors are combined into energy spectra, pitch-angle distributions, differential and integral flux intensities and mean particle energies for both the electron and proton fluxes. The program also generates a new condensed magnetic tape record of the outputs of the selected detectors for the chosen time intervals and allows the storage of many of these interesting time intervals from different orbits on one tape for convenience and economy in further processing. The program subdivides each interval into 100-second periods and for each 100-second period it produces eight separate plots, prints an output record of all computed and plotted quantities, and

produces a microfilm copy of both the plots and the printed outputs. Some of the computer plots giving the electron results for a representative period are shown in Figures 4.5, 4.6 and 4.7. The satellite is in the southern dayside auroral zone heading north (at a magnetic latitude of about 70°). The abscissa is a continuously running time index (in seconds). The left-hand section of Figure 4.5 shows the results from the nominal 0° CME detectors. The curve between 1 and 2 on the ordinate scale is the logarithm of the integral of the electron flux between 0.8 and 16.3 keV obtained from the CME-1 detectors. It varies between 10^6 and 10^{10} electrons/cm^2-sec-steradian in the interval indicated. The solid curve between 0 and 1 on the ordinate gives the average electron energy on a linear scale in keV (between 0 and 20 keV). The dotted curve gives the orientation; that is, the pitch angle being sampled by this set of detectors, on a linear scale between 0° (ordinate = 0) and 180° (ordinate = 1.8). The region of the plot between 2 and 7 on the ordinate scale contains the differential electron spectrum from the CEM-1 detectors for each second of the period illustrated when the flux was significantly above background. The spectrum from the first second is the plot at the top left, the next is one plot down and etc. The spectra have been normalized to one unit of ordinate, and two decades are plotted on a logarithmic scale. In examining these data shown in Figure 4.5, one sees two regions of significant fluxes, the second one being harder and more intense.

The right-hand section of Figure 4.5 shows a similar set of plots for the CME-2 and CME-3 detectors (nominal 55° pointing direction). Figure 4.6 shows similar results for the CME-4 (nominal 90° pointing direction) and CME-5 (nominal 180° pointing direction) detectors. The integral electron fluxes measured at the various pitch angles corresponding to the instantaneous pointing directions of these several instruments are gathered together in Figure 4.7 where a pitch-angle distribution at each second of the period illustrated is plotted. The distribution from the first second is the plot at the top left. The next is one plot down, etc. The abscissa of each plot is pitch angle in degrees (20° per subdivision). The ordinate is the logarithm of the integral flux varying from 10^5 to 10^{10} electrons/cm^2-sec-ster. One sees that during the events shown the flux was roughly isotropic in the

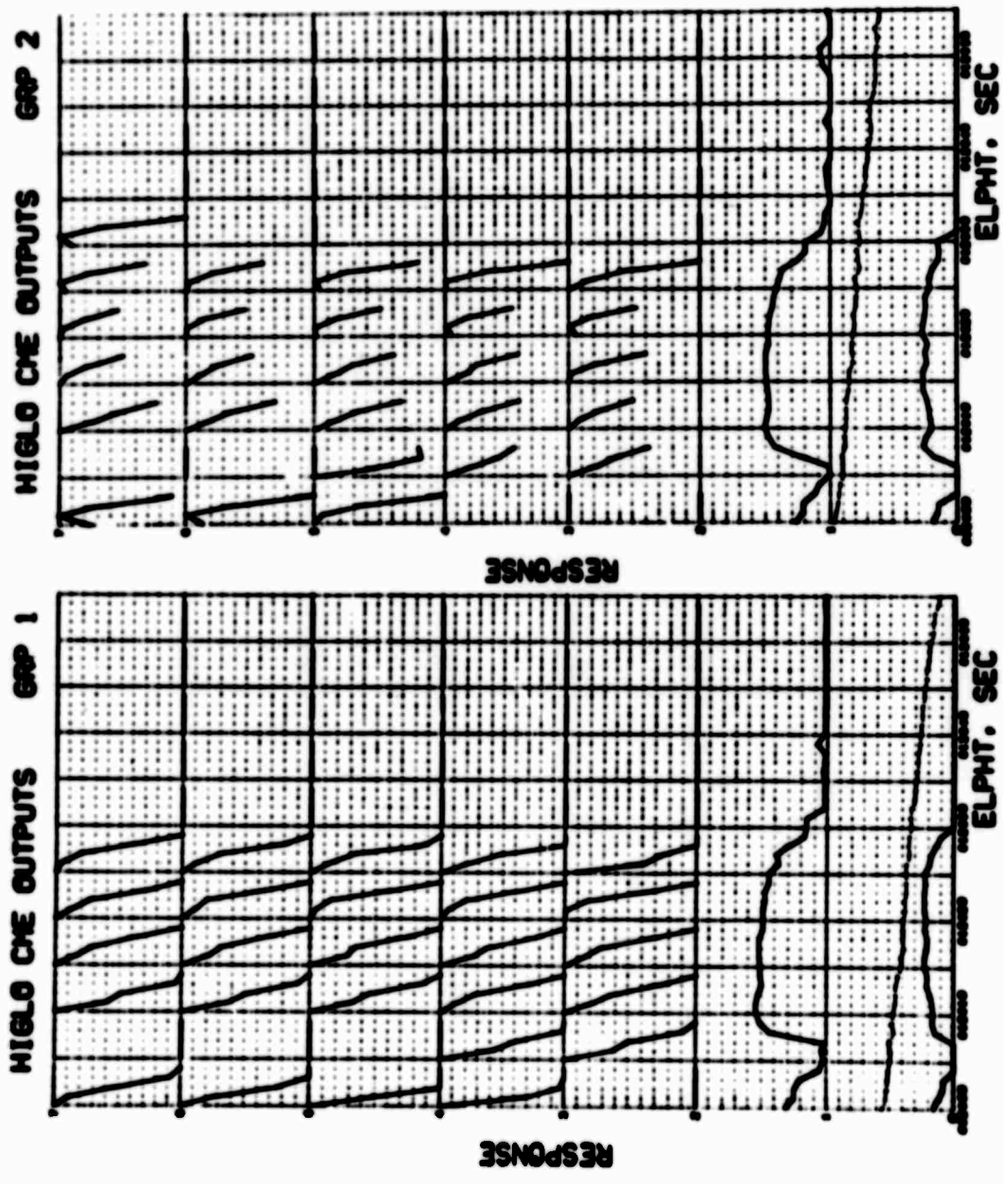

Figure 4.5 Electron fluxes during a traversal of the southern dayside auroral zone on 13 May 1969.

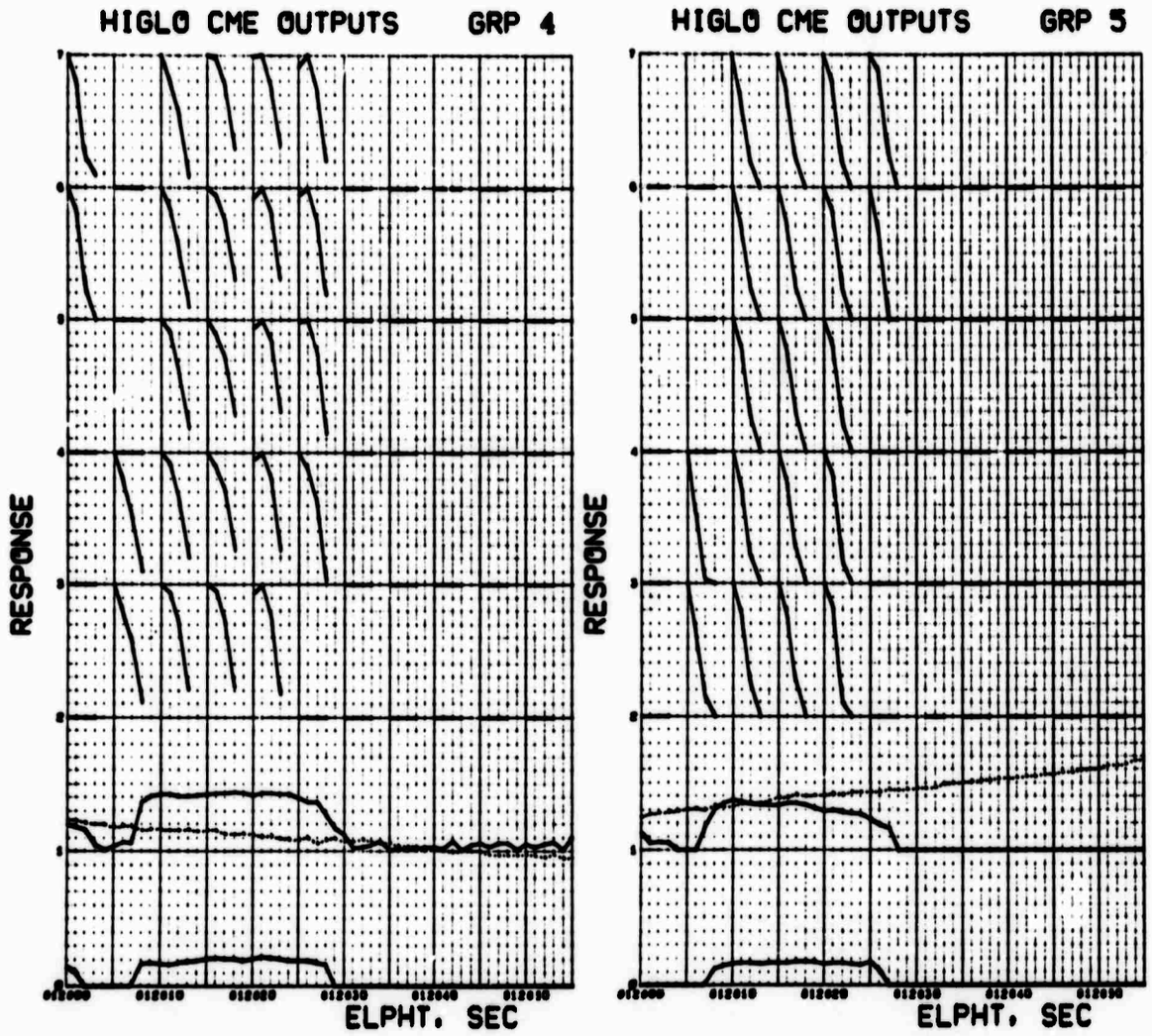

Figure 4.6 Electron fluxes during a traversal of the southern dayside auroral zone on 13 May 1969.

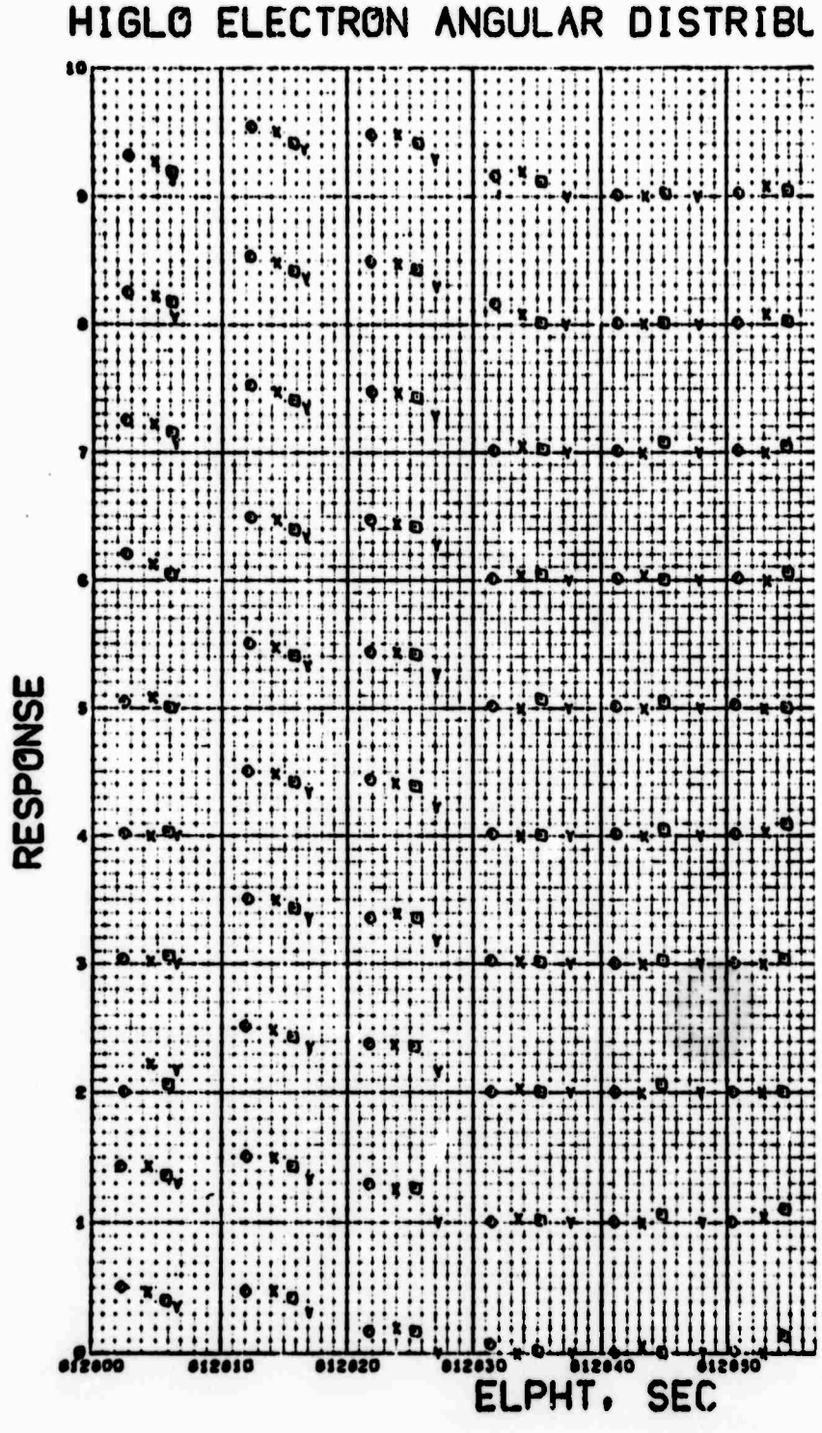

Figure 4.7 Electron angular distributions during a traversal of the southern dayside auroral zone on 13 May 1969.

upper hemisphere, while the upward traveling (backscattered) flux was substantially reduced.

The next step in the analysis is the quantitative intercomparison of the electron and proton fluxes as computed by the previously-described program with the various ionospheric measurements made simultaneously on the satellite. This step has not yet been accomplished since the correct satellite orbital elements which are to be supplied by the Air Force have not been received for revolutions below 389.

The ephemeris program routinely used in conjunction with the data analysis makes use of the inertial coordinates provided on an hourly basis by ENT Air Force Base, Colorado. The program represents a modification of one previously written at LMSC. In addition to providing the geographic coordinates once every ten seconds, several other important quantities are computed. Subroutines are incorporated for calculating various quantities relating to the earth's magnetic field: B,L, the invariant latitude, K_{Min}, altitude of the conjugate point, and the auroral time. For a typical orbit acquisition approximately two to three minutes of 1108 computer time is required.

After the ephemeris is generated for a given orbit, certain tests are routinely performed to verify its validity. In one of the mose useful of these checks, the current outputs of the solar cell arrays are compared with the times of transition from lightness to darkness, as calculated in the ephemeris program. This test can be performed to an accuracy of 3 to 5 seconds. Additional information on the onset times of lightness and darkness is obtained from the solar sensors. Another validity check involves comparisons between the magnetic field strengths measured with the magnetometer and those calculated from the geographic position and the earth's magnetic field model. This technique will readily indicate the existence of large errors in the ephemeris but is not competitive with the light sensors in regard to accuracy. The response of the IVM instrument to the four crossings of the outer radiation belt on each orbit also serves as an indication of any gross ephemeris errors.

As a result of the foregoing tests it was discovered that the ephemeris values supplied by ENT Air Force Base were in serious error for the first 388 orbits. For example, on orbit 388 the light sensor indicated a time equivalent error of 125 seconds. Upon further checking, a sudden step function in the satellite position, as derived from the ephemeris cards supplied by ENT, was uncovered. It is now generally agreed that the tracking data used were for another object near the OV1-18 satellite. Accordingly, for the last six months personnel at ENT have been trying without success to generate a correct ephemeris for the first 388 orbits. As a result of their difficulties, attempts are now being made at LMSC to run valid ephemeris for orbits greater than 388 "backward" in time for about 20 days to cover the earlier orbits.

Recently, the accuracy of the ephemeris has been tested for revolution 6007 by comparing the calculated positions with those measured with radar techniques by Dr. A. Freed at Lincoln Laboratory, Massachusetts Institute of Technology. The calculated and measured positions were found to agree within five kilometers.

As originally designed, all of the charged particle detectors were to maintain a constant orientation with respect to the zenith and the vehicle velocity direction. Under these conditions the detector orientation with respect to the local magnetic field direction would be readily calculable from established magnetic field models and the satellite ephemeris. However, because of the failure of the gravity-gradient stabilization system and the resultant tumbling of the vehicle, the detector orientations must be calculated from the on-board magnetometer measurements. The calculated orientation of the instruments is very sensitive to the corrections to the measured field which must be applied because of vehicle fields. If one assumes that the vector offset field is constant in the frame of the satellite, it can be determined by comparing the measured field with the field expected on the basis of established field models. If we define the quantities

$$B_O = \text{Model field}$$
$$B_M = \text{Measured field}$$
$$\Delta_B = B_M - B_O$$

an offset field will show up as a quasi-periodic modulation of ΔB with a period equal to the spin period of the satellite. This is clearly demonstrated in Figure 4.8. The modulation is not a simple sinusoidal function because the vector orientation of the vehicle offset field and the geomagnetic field varies in a complex way as the satellite tumbles.

If one assumes a possible vehicle offset field with vector components $-C_j$ where j deonted the coordinate axis and an error in the calibration scale factor of (A_2-1) for each axis, we can relate the true (model) field B_j to the measured field b_j in the following way.

$$B_j(t) = A_j[b_j(t) + C_j]$$

If the vehicle orientation were independently known, one could calculate $B_j(t)$ from the model and evaluate C_j and A_j from a best fit. However, without prior knowledge of the vehicle orientation we must base our corrections on the discrepancy in the total field.

$$B(t) = \left(A_1^2[b_1(t)+C_1]^2 + A_2^2[b_2(t)+C_2]^2 + A_3^2[b_3(t)+C_3]^2\right)^{\frac{1}{2}}$$

To evaluate C_1, we first choose cases where $b_2(t_i) = b_3(t_i) = 0$, in which case we can write

$$B_i = \left\{ A_1^2(b_{1i}+C)^2\left[1+\left(\frac{A_2C_2}{A_1[b_{1i}+C_1]}\right)^2 + \left(\frac{A_3C_3}{A_1[b_{1i}+C_1]}\right)^2\right]\right\}^{\frac{1}{2}}$$

where we have used the notation $B(ti) \equiv B_i$ and $b_1(t_i) = b_{1i}$. If, as is shown to be the case, the corrections are small compared with the total field, we can drop the second order terms and obtain

$$B_i \cong A_1(b_{1i} + C_1).$$

From two such cases, one where $b_{1j} > 0$ and the other where $b_{1k} < 0$, we have

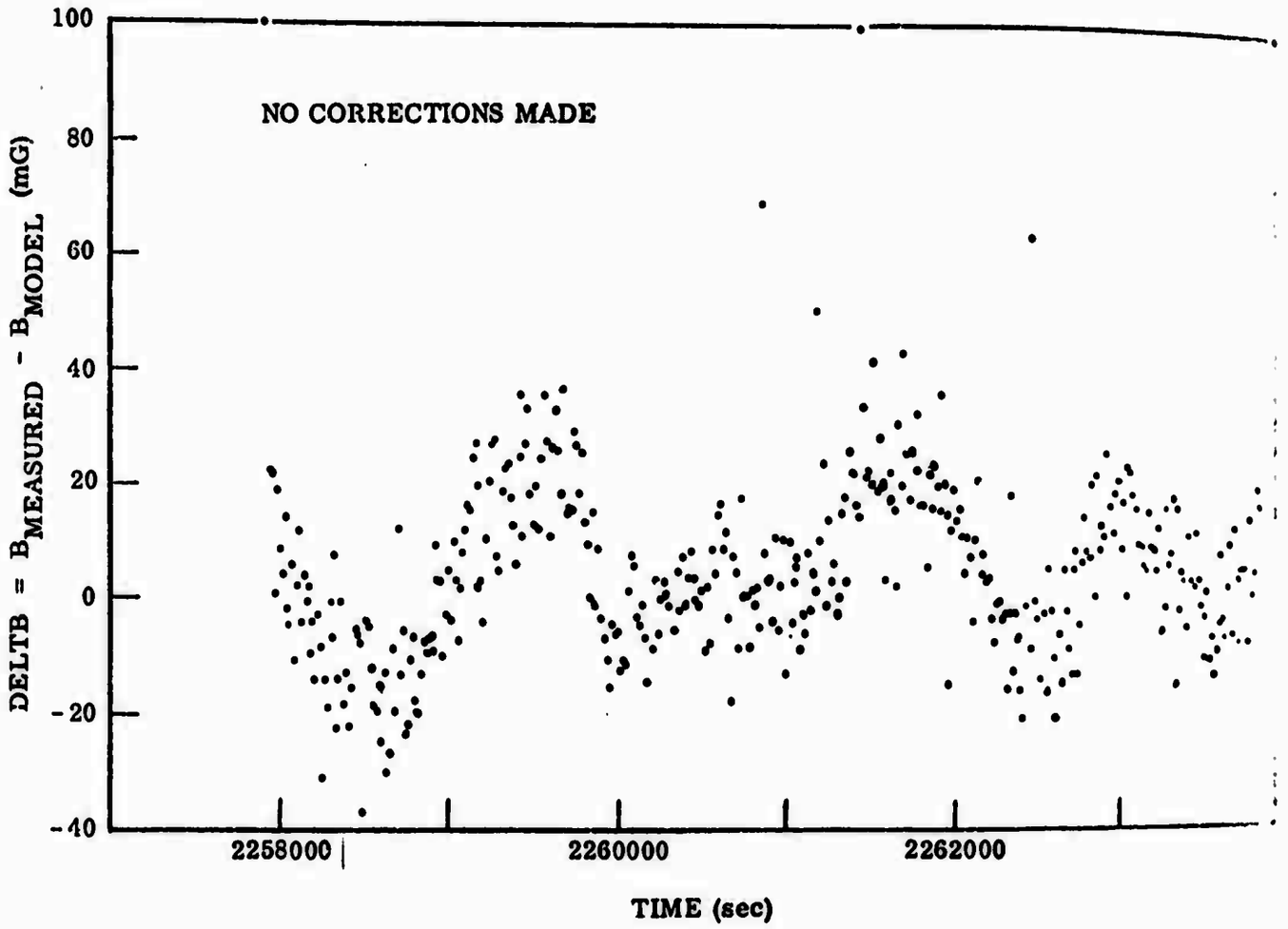

Figure 4.8 The effects of magnetic field offsets on the magnetometer data (uncorrected).

$$B_k = -A_1(b_{1k}+C_1) = A_1(|b_{1k}|-C_1)$$

$$B_i = A_1(b_{1k}+C_1) .$$

Then

$$A_1 = \frac{B_i + B_k}{b_{1i} + |b_{1k}|}$$

$$C_1 = \frac{B_i|b_{1k}| - B_k b_{1i}}{B_i + B_k} .$$

Similar results obtained for A_2,C_2 and A_3,C_3 by choosing suitable cases where $b_1 = b_3 = 0$ and $b_1 = b_2 = 0$, respectively.

A statistical analysis of all available data for these cases lead to the following results.

$$C_R = -19 \text{ mG}$$

$$C_V = -\ 8 \text{ mG}$$

$$C_Z = -\ 9 \text{ mG}$$

$$A_R \tilde{=} A_V \tilde{=} A_Z \tilde{=} 1.02$$

Figure 4.9 is the same data shown in Figure 4.8 after correcting for the offset field, but not applying the scale factor. The solid line shows where the zero line would be if a scale correction A = 1.025 were applied to the data. It is obvious that the periodic modulation has been eliminated. The remaining scatter results primarily from the finite resolution of the telemetry system and general noise.

The analysis of the ion density has not at present been undertaken other than to verify the proper operation of the IEA instrument and to demonstrate that significant horizontal ion gradients do exist in the ionosphere. A typical portion of these results are shown in Figure 3.2 and has been described

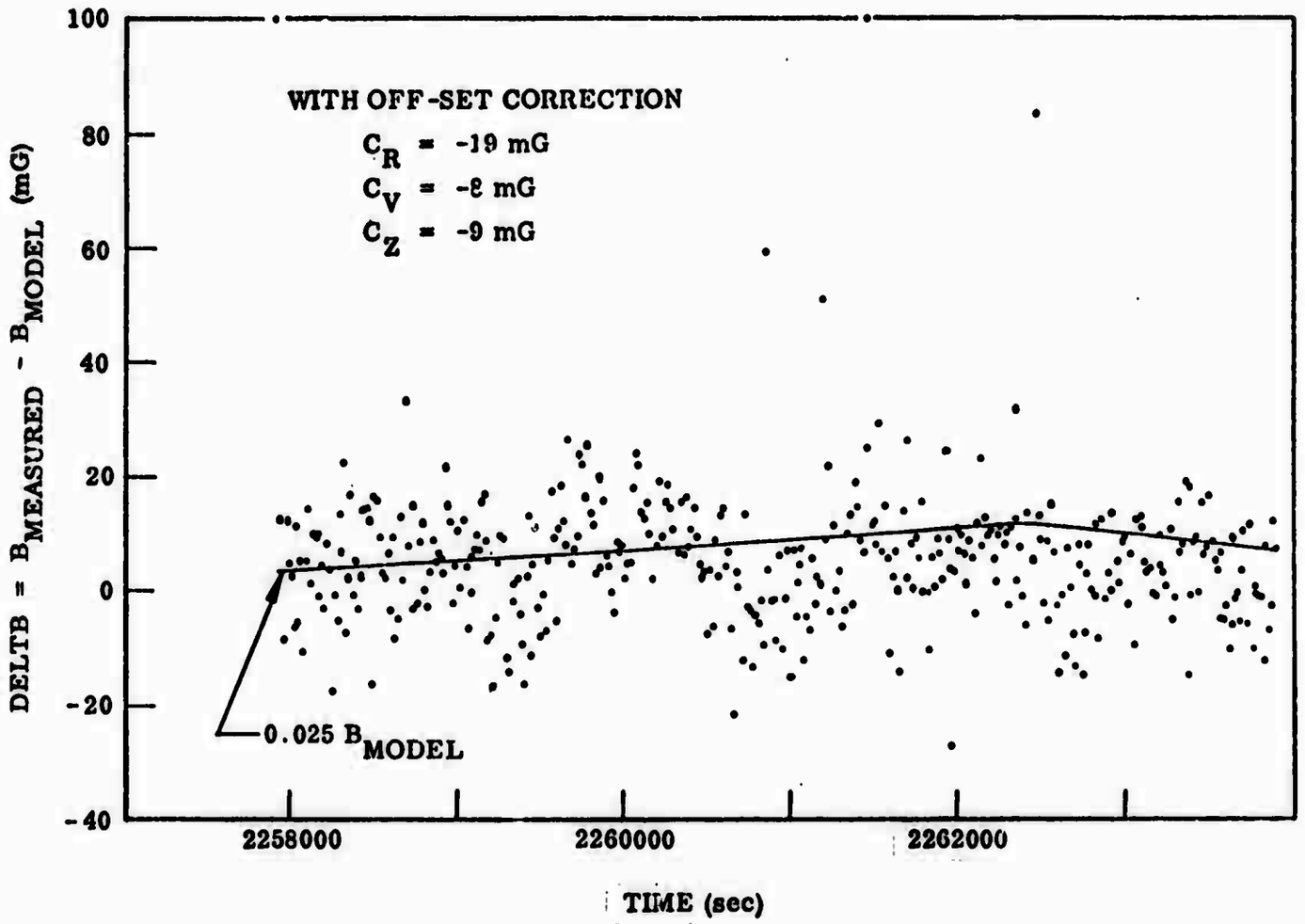

Figure 4.9 The effects of magnetic field offsets on the magnetometer data (corrected).

in an earlier section. The detailed analysis of the ion density requires accurate information as to the orientation of the sensor elements to the direction of the velocity vector. At present the attitude-orbit information has not been supplied by the Air Force. As the attitude data becomes available the processing of the ion density data will proceed.

As has been indicated, the vehicle did not achieve even the predicted two-axes stabilization and was in a variable period tumbling mode. This vehicle motion will significantly complicate the analysis of the ion density and the ion temperature.

The analysis of the electron density and temperature data from the cylindrical Langmuir probe is much less dependent upon the vehicle orientation. Consequently, some progress has been made toward the electron density and temperature analysis on a first-look basis. The tumbling mode of the vehicle will, however, affect the electron density and temperature analysis in that for certain periods the probe will be in the wake of the vehicle. While in the wake, the electron density measured by the probe is not simply related to the undisturbed electron density. Consequently, the orientation of the vehicle must be known to insure proper interpretation of the electron data.

Preliminary analysis of EEA data has revealed several interesting results, particularly with regard to the fluxes of electrons in the energy range 0-10 eV. Figure 4.10 illustrates two energy spectra recorded at night, one in the equatorial region and the other in the auroral region. The large fluxes of electrons at night with energy in the 0-2, 2-4 and 4-8 eV range at the equatorial region are unexpected. A plausible source of excitation for such large fluxes is not known at present. These fluxes of electrons may contribute to the stable red arcs observed from ground stations during the same general period.

The value of the data is somewhat decreased and the difficulty of analysis increased by the tumbling of the spacecraft. The sensors were optimally oriented with respect to the planned stable orientation of the space platform. However, significant results are still expected.

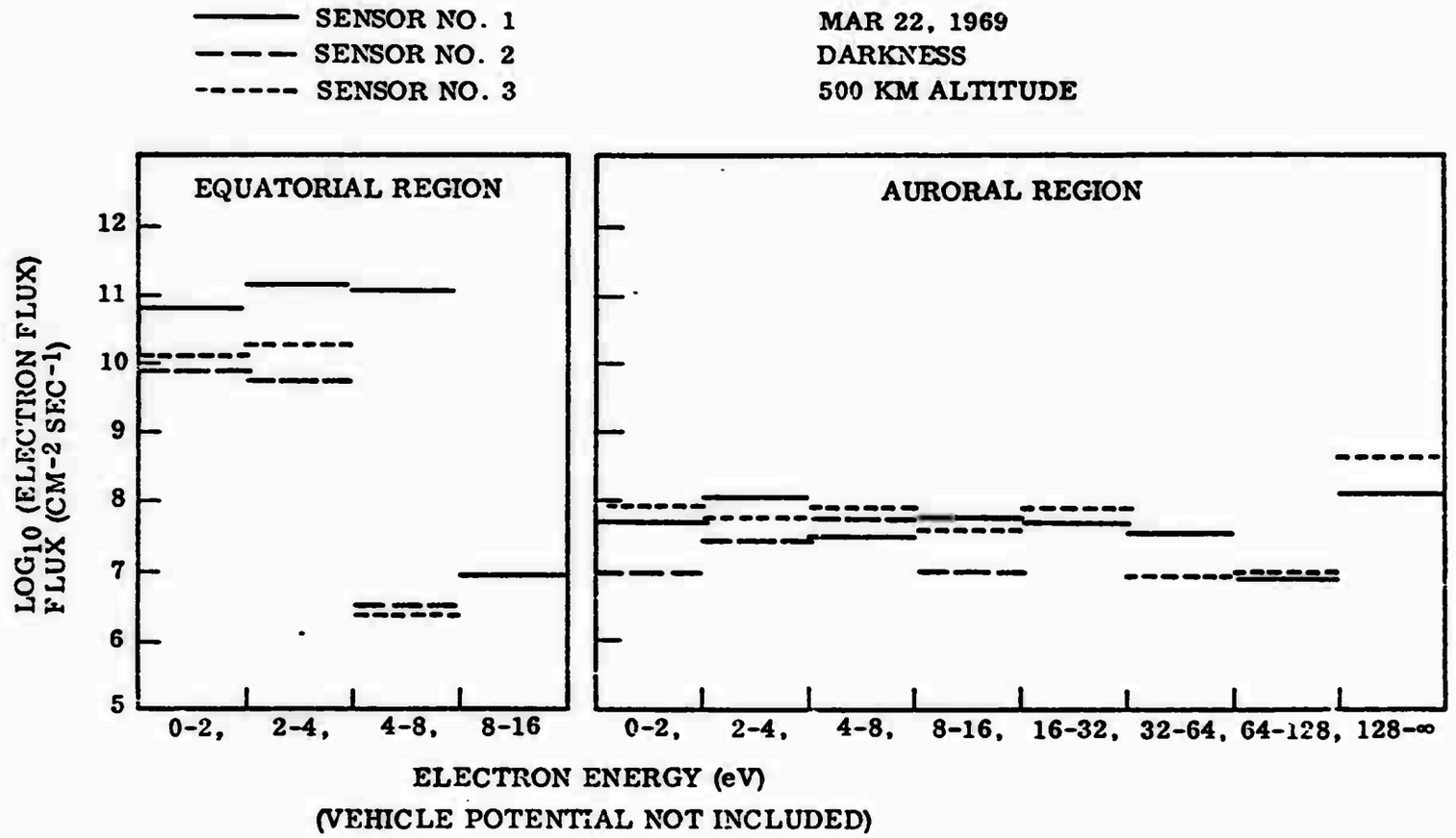

Figure 4.10 Energy spectra from the epithermal electron analyzer.

Section 5

SUMMARY AND CONCLUSIONS

The principle conclusion is that in spite of the failure of the satellite to achieve orientation, all of the instruments provided some high-quality data and a large body of data has been acquired that promises to yield significant results on the systematic relationships between the ionospheric structure at this altitude and the input energy in the form of particle fluxes. The Langmuir probe functioned well throughout the experiment and the Ion Energy Analyzer functioned well during the first 225 orbits. They have demonstrated that ionospheric structure is observed and is significant at this altitude and have provided a body of data sufficient for a detailed intercomparison with the particle detectors. The failure of the vehicle to achieve stabilization has complicated the analyses and the delay in obtaining good ephemeris data for the period prior to orbit 388 has resulted in a delay in the analysis of the ion and electron density results since detailed attitude information is required for the interpretation of the data.

Substantial progress in the analysis of the particle data has been achieved in spite of the added complications due to the vehicle tumble. A series of computer programs has been written, the successful performances of the instruments has been established, and detailed surveys of the particle fluxes for some of the early orbits has been performed. We are confident that the intercomparison of these fluxes with the ionospheric structure results when they become available will yield new insight into the causes of ionospheric structures in this altitude regime.

UNCLASSIFIED

Security Classification

DOCUMENT CONTROL DATA - R & D

(Security classification of title, body of abstract and indexing annotation must be entered when the overall report is classified)

1. ORIGINATING ACTIVITY *(Corporate author)*

Lockheed Palo Alto Research Laboratory

2a. REPORT SECURITY CLASSIFICATION

UNCLASSIFIED

2b. GROUP

3. REPORT TITLE

INVESTIGATION OF HORIZONTAL ION DENSITY GRADIENTS IN THE IONOSPHERE

4. DESCRIPTIVE NOTES *(Type of report and inclusive dates)*

Final Technical Report, 15 July 1965 through 29 May 1970

5. AUTHOR(S) *(First name, middle initial, last name)*

Gerald W. Sharp, Richard D. Sharp and Richard G. Johnson

6. REPORT DATE	7a. TOTAL NO. OF PAGES	7b. NO. OF REFS
May 1970	75	9

8a. CONTRACT OR GRANT NO.	9a. ORIGINATOR'S REPORT NUMBER(S)
NOnr 4969(00)	LMSC/L-39-70-1
b. PROJECT NO.	
c.	9b. OTHER REPORT NO(S) *(Any other numbers that may be assigned this report)*
d.	

10. DISTRIBUTION STATEMENT

This document has been approved for public release and sale; its distribution is unlimited.

11. SUPPLEMENTARY NOTES	12. SPONSORING MILITARY ACTIVITY
	Office of Naval Research Advanced Research Projects Agency

13. ABSTRACT

This final report is on a satellite measurement program to investigate the characteristics and causes of horizontal ion density gradients in the F-region ionosphere. The report covers the development of the payload, the satellite orbital operations, and the preliminary data analysis phase of the program. The satellite payload was successfully launched on the OV1-18 satellite on 18 March 1969 into a polar orbit with apogee at 590 km and perigee at 469 km. The payload performed generally well throughout the first year's operation although the satellite failed to achieve the desired earth-centered orientation. A large body of generally high-quality flight data has been acquired that promises to yield significant results on the systematic relationships between the ionospheric structure at the satellite altitude and the input energy sources in the form of energetic particle fluxes. Electron density and temperature measurements with a Langmuir probe were acquired during the first 225 orbits. The preliminary data analysis has shown that ionospheric structure is observed and is significant. Computer programs for processing the flight data have been developed and are discussed. The computer programs have been used to perform detailed surveys of the particle fluxes for some early orbits.

This research was supported by the Advanced Research Projects Agency (ARPA Order 215) and was conducted under Office of Naval Research Contract NOnr 4969(00), Task No. 321-009.

DD FORM 1 NOV 65 1473

UNCLASSIFIED

Security Classification

14. KEY WORDS	LINK A		LINK B		LINK C	
	ROLE	WT	ROLE	WT	ROLE	WT
Ionosphere						
Ion density gradients						
Ionospheric structure						
Satellite instrumentation						
OV1-18 satellite						